



Tech Briefs

National Aeronautics and
Space Administration



Electronic Components and Circuits



Electronic Systems



Physical Sciences



Materials



Computer Programs



Mechanics



Machinery



Fabrication Technology



Mathematics and Information Sciences



Life Sciences

Am 2002 005864

INTRODUCTION

Tech Briefs are short announcements of innovations originating from research and development activities of the National Aeronautics and Space Administration. They emphasize information considered likely to be transferable across industrial, regional, or disciplinary lines and are issued to encourage commercial application.

Availability of NASA Tech Briefs and TSPs

Requests for individual Tech Briefs or for Technical Support Packages (TSPs) announced herein should be addressed to

National Technology Transfer Center

Telephone No. (800) 678-6882 or via World Wide Web at www2.nttc.edu/leads/

Please reference the control numbers appearing at the end of each Tech Brief. Information on NASA's Commercial Technology Team, its documents, and services is also available at the same facility or on the World Wide Web at www.nctn.hq.nasa.gov.

Commercial Technology Offices and Patent Counsels are located at NASA field centers to provide technology-transfer access to industrial users. Inquiries can be made by contacting NASA field centers and program offices listed below.

NASA Field Centers and Program Offices

Ames Research Center
Carcine Blake
(650) 604-1754 or
cblake@mail.arc.nasa.gov

Dryden Flight Research Center
Lee Duke
(805) 258-3802 or
lee.duke@dfrc.nasa.gov

Goddard Space Flight Center
George Alcorn
(301) 266-5810 or
galcorn@gsc.nasa.gov

Jet Propulsion Laboratory
Merle McKenzie
(818) 354-2577 or
merle.mckenzie@jpl.nasa.gov

Johnson Space Center
Hank Davis
(281) 463-0474 or
henry.l.davis1@jsc.nasa.gov

John F. Kennedy Space Center
Gale Allen
(407) 867-6226 or
gale.allen-1@ksc.nasa.gov

Langley Research Center
Sam Morello
(757) 864-8005 or
s.a.morello@lerc.nasa.gov

Glenn Research Center
Larry Vitens
(216) 433-3484 or
cto@grc.nasa.gov

George C. Marshall Space Flight Center
Sally Little
(256) 544-4266 or
sally.little@msfc.nasa.gov

John C. Stennis Space Center
Kirk Sharp
(228) 688-1909 or
technology@ssc.nasa.gov

NASA Program Offices

At NASA Headquarters there are seven major program offices that develop and oversee technology projects of potential interest to industry:

Carl Ray
Small Business Innovation
Research Program (SBIR) &
Small Business Technology
Transfer Program (STTR)
(202) 358-4652 or
cray@mail.hq.nasa.gov

Dr. Robert Norwood
Office of Commercial Technology
(Code RW)
(202) 358-2320 or
rnorwood@mail.hq.nasa.gov









John Mankins
Office of Space Flight (Code MP)
(202) 358-4659 or
jmankins@mail.hq.nasa.gov

Terry Hertz
Office of Aero-Space Technology
(Code RS)
(202) 358-4636 or
thertz@mail.hq.nasa.gov

Glen Mucladow
Office of Space Sciences
(Code SM)
(202) 358-2235 or
gmuckdow@mail.hq.nasa.gov

Roger Crouch
Office of Microgravity Science
Applications (Code U)
(202) 358-0689 or
rcrouch@hq.nasa.gov

Granville Paulsen
Office of Mission to Planet Earth
(Code Y)
(202) 358-0706 or
gpaules@mtpe.hq.nasa.gov

- | | | |
|-----------|---|---|
| 5 | Electronic Components and Circuits |  |
| 11 | Electronic Systems |  |
| 17 | Physical Sciences |  |
| 25 | Materials |  |
| 31 | Mechanics |  |
| 37 | Machinery |  |
| 41 | Fabrication Technology |  |
| 45 | Mathematics and Information Sciences |  |

This document was prepared under the sponsorship of the National Aeronautics and Space Administration. Neither the United States Government nor any person acting on behalf of the United States Government assumes any liability resulting from the use of the information contained in this document, or warrants that such use will be free from privately owned rights.

4

BLANK PAGE



Electronic Components and Circuits

Hardware, Techniques, and Processes

- 7 Readout for Fast IR Imaging With Large Detector Capacitance
- 8 Flip-Chip W-Band Amplifier: a Prototype of Q-MMICs
- 8 Nonsaturating Electronic Image Sensors

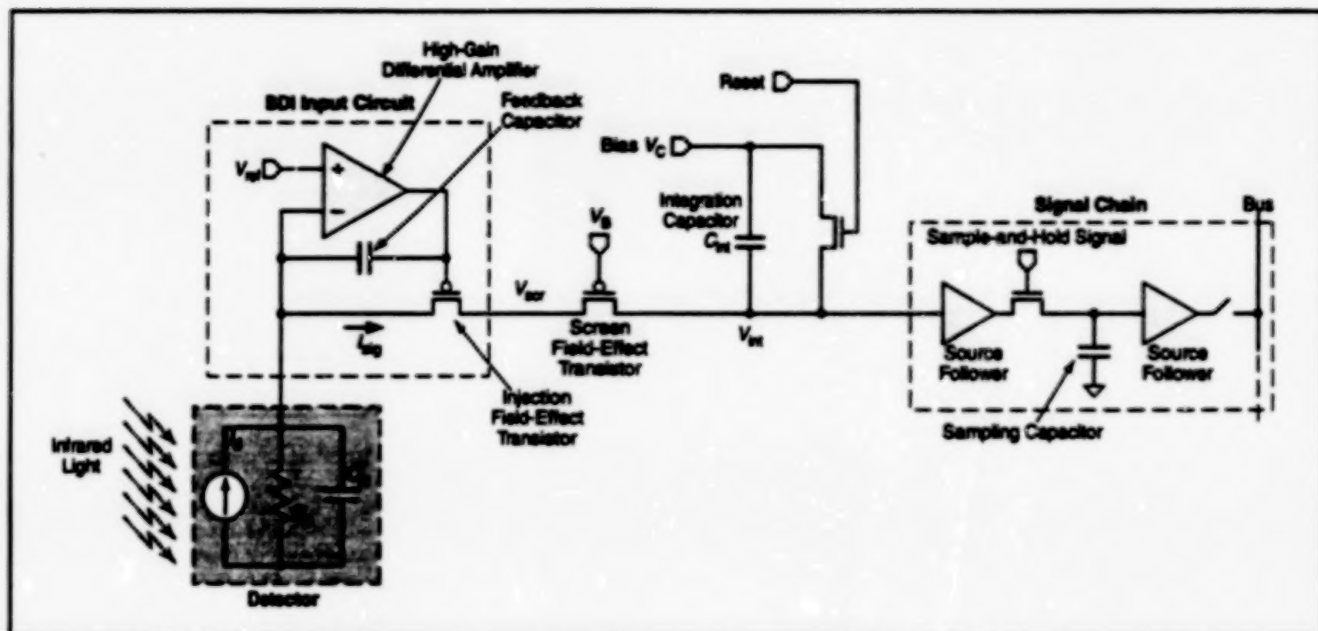
6

BLANK PAGE

Readout for Fast IR Imaging With Large Detector Capacitance

Improvements are effected by taking account of response times in designing readout amplifiers.

NASA's Jet Propulsion Laboratory,
Pasadena, California



The Stages Following the BDI Input Circuit are optimized, pursuant to equations for response times, to minimize image lag and other errors.

A methodology for designing highly accurate readout circuits for infrared (IR) image detectors that have large pixel detector capacitances (of the order of tens of picofarads) and are required to operate with short exposure times ($<100 \mu s$) has been devised. In this context, "highly accurate" signifies capable of (1) nearly linear response over a wide dynamic range with (2) little or no image lag ("ghost" image readout attributable to capacitive retention of charge from preceding image frames), and (3) low readout noise. The methodology has been used to enhance the performance of NASA's Airborne Visible/Infrared Imaging Spectrometer (AVIRIS), and is expected to satisfy an increasing need for highly accurate readout circuits in other applications, including other imaging spectrometers and infrared video cameras now undergoing development.

The methodology improves upon the prior art in two main ways:

- It provides for refinement of the design of pixel amplifiers and other pixel readout circuitry on the basis of understanding gained through analysis of previously neglected second-order electronic effects — including notably image lag related to abrupt transitions

of signal currents.

- It incorporates the concept that, at least in principle, it should be possible to derive an algorithm to correct for image lag.

The readout circuitry for each pixel, as contemplated in this methodology, is based on that of the AVIRIS. This circuitry (see figure) features a conventional buffered-direct-injection (BDI) input circuit followed by amplifier stages of optimized design. Similar BDI readout circuits designed according to older methodology generate residual image signals when bright images are followed by dark images, giving rise to errors in the estimates of the dark images; and when dark images are followed by bright images, responses are oscillatory, giving rise to errors in estimates of the bright images. The errors are functions of time and detector capacitances.

The analysis of second-order effects yields closed-form expressions for response times for both low-to-high and high-to-low transitions. These expressions are what make it possible to optimize pixel amplifier design and to choose appropriate feedback capacitors to minimize circuit error and image lag. In an initial application of this part of the methodology to a linear array of photodiodes for the AVIRIS, it was found that

the signal-to-noise ratio was increased by a factor of 2 to 3, relative to older designs, and that image lag was reduced to less than 10 percent over the entire dynamic range of pixel signal current from 10 pA to 10 nA. The measured input-referred noise was found to be less than 300 electrons.

A first-order analysis has been performed in an initial effort to develop software to compensate for image lag. This analysis yields recursive equations that can be used to estimate and correct for errors. Software that implements these equations has been tested on AVIRIS readout data and found to reduce errors but also to occasionally introduce new errors. The inability to eliminate all errors has been attributed to inadequate mathematical modeling of circuit behavior, including inaccuracies in estimates of response times. To achieve greater accuracy, it would be necessary to derive equations of greater complexity, based on a second-order analysis. Of course, it would be more difficult to implement such equations in software.

This work was done by Bedabrata Pain of Caltech for NASA's Jet Propulsion Laboratory. Further information is contained in a TSP [see page 1].
NPO-20522

Flip-Chip W-Band Amplifier: a Prototype of Q-MMICs

Q-MMICs offer an economical alternative to MMICs.

A prototype W-Band, low-noise amplifier has been fabricated by bump-bonding a high-speed, low-noise InP high-electron-mobility (HEMT) transistor onto the previously fabricated passive portion of the amplifier circuit on a GaAs substrate (see figure). The passive portion of the circuit can be regarded as a monolithic microwave integrated circuit (MMIC) that differs from a complete MMIC amplifier only in its lack of a single active device (the HEMT). Therefore, the bump-bonded combination of the active device and the passive portion of the circuit is characterized as a quasi-monolithic millimeter-wave integrated circuit (Q-MMIC).

Heretofore, it has been necessary to resort to expensive custom fabrication of MMICs to satisfy requirements for special-purpose millimeter- and submillimeter-wave circuits that have not been commercially available. In comparison with MMICs, Q-MMICs offer the potential advantages of lower cost and greater design flexibility, in the following respects:

- Part of the reduction in cost is attributable to the conservation of expensive semiconductor area for the fabrication of active devices, in conjunction with the use of cheaper substrates for the more expensive passive circuitry.
- One can ensure higher circuit overall performance and production yield by testing components prior to assembly and bonding.
- This approach affords the flexibility to mix and match discrete active devices with more-easily-fabricated passive circuits and circuit components to create custom high-performance circuits.
- Because the discrete active devices and the passive circuits are fabricated separately, the subprocesses for fabricating each component can be less

An InP HEMT like the one shown at the top was bump-bonded onto the passive portion of the amplifier circuit. Near the center of the passive circuitry are six Au/Sn bumps for fluxless bonding with the HEMT. The six marks on the contact pads are not bonding bumps but, rather, marks left by routine screening with water probes.

complex, and thus the overall fabrication process can be simplified.

- By bump bonding, one can hybridize the best-available active devices with passive circuits. In so doing, one can take advantage of (1) the flexibility afforded by the use of discrete microwave integrated circuits, (2) the performance advantage of MMIC's, (3) short design and fabrication times, (4) low costs of fabrication, and (5) uncompromised frequency performance.

In order to make the present flip-chip (bump-bonding) approach viable, it was necessary to solve two major problems. The first problem was to minimize para-



HEMT



PASSIVE PORTION OF AMPLIFIER CIRCUIT

NASA's Jet Propulsion Laboratory,
Pasadena, California

sitic millimeter-wave resonances associated with the metal bonding bumps. The solution of this problem was simply to make the bumps smaller than they had been made previously. The reduction in parasitic resonances associated with the bumps enables the amplifier circuit to operate at higher frequencies.

The other problem was to make it possible to handle the HEMTs by use of a conventional vacuum chuck. These particular HEMTs were small enough to pass through the vacuum hole in the collet on the vacuum chuck. It was necessary to fabricate a collet adapter with a vacuum hole only 50 μm wide; because a bit for drilling such a narrow hole does not exist, the collet adapter was micromachined from silicon. The collet adapter was also refined by making the hole in a pedestal on which several discrete devices could be held closely together for bump bonding onto the same circuit. This refinement makes it possible to assemble more complex circuits that contain multiple discrete devices — for example, a multistage amplifier.

In a performance test covering the frequency range from 85 to 120 GHz, the prototype W-band amplifier was found to operate with a peak gain of about 6 dB at a frequency at 91 GHz, falling off to about 0 dB at 117 GHz. The highest previously published operational frequency for an amplifier fabricated by bump bonding a discrete active device onto a passive circuit was about 60 GHz.

This work was done by Paul Pinsukanjana, Lorene Samoske, Todd Gaier, R. Peter Smith, Alexander Ksendrov, Michael Rusimmons, and Suzanne Martin of Caltech and Richard Lai of TRW for NASA's Jet Propulsion Laboratory. Further information is contained in a TSP [see page 1], NPO-20650

Nonsaturating Electronic Image Sensors

In each pixel, charge would be integrated as long as necessary, but not longer.

Focal-plane electronic image sensors that would not saturate when exposed to intense illumination have been proposed. These sensors could be used to acquire accurate, scientific-quality data on images (including spectral images), even when the images contain both very bright and very

dark areas. The proposed sensors would not contain automatic gain-control (AGC) circuitry, yet their dynamic ranges would exceed those of sensors with AGC. Unlike AGC circuitry, the circuitry of the proposed sensors would not change noise levels and would not compress image data.

NASA's Jet Propulsion Laboratory,
Pasadena, California

The proposed sensors would be of the active-pixel-sensor (APS) type. The designs of these sensors would exploit the possibility of making APS circuitry operate on each pixel individually during acquisition of image data. In particular, the amount of photocharge accumulat-

ed in each pixel during each exposure would be monitored, and the pixel would be either reset or turned off when the charge increased beyond a preset threshold.

In one suggested implementation, a comparator and a counter would be added to the readout circuit of each pixel. When the amount of charge reached the preset threshold during an exposure, the pixel would be reset and the count incremented by one. At the end of the exposure, the total readout signal charge for each pixel would be the sum of (1) the number of resets \times the threshold charge plus (2) the charge accumulated since the last reset. In the presence of bright light, the repeated resets would prevent saturation. In the

presence of dim light, the photocharge would be allowed to grow for as long a time as necessary during an exposure.

In another suggested implementation, the readout circuitry for each pixel would include a sample-and-hold circuit. In this case, the pixel value would be captured whenever the sampled photocharge exceeded a preset threshold and the integration time counted separately. In either implementation, it may be possible to obtain satisfactory performance while using an analog-to-digital converter of fewer bits than would ordinarily be needed for a given dynamic range.

This work was done by Gregory Beaman, Bedabrata Pain, and Robert Stibel of Caltech for NASA's Jet Propulsion

Laboratory. Further information is contained in a TSP [see page 1].

In accordance with Public Law 96-517, the contractor has elected to retain title to this invention. Inquiries concerning rights for its commercial use should be addressed to

Technology Reporting Office

JPL

Mail Stop 122-116

4800 Oak Grove Drive

Pasadena, CA 91109

(818) 354-2240

Refer to NPO-20580, volume and number of this NASA Tech Briefs issue, and the page number.



Electronic Systems

Hardware, Techniques, and Processes

- 13 Data-Filter Algorithm for Monitoring a Power System
- 13 Automated Apparatus for Testing Gyroscopes
- 15 System Locates Lightning Strikes to Within Meters
- 16 Portable ECG/EGG Data Recorder

Data-Filter Algorithm for Monitoring a Power System

In the manner of human experts, redundancy is utilized to detect anomalies.

Lyndon B. Johnson Space Center,
Houston, Texas

An algorithm has been developed for a computer-based electronic system that would aid human ground controllers in monitoring data from sensors in the electric-power system of the International Space Station. Among other things, the algorithm encodes knowledge of human experts; thereby harnessing the ability of computers to do diagnostic calculations that human experts would do but that take much longer when done manually. The algorithm also has potential for application to a variety of systems outside the aerospace industry.

The Space Station power system is characterized by two levels of redundancy: (1) two or more sensors measure the same value; and (2) synthetic (probable) measurements can be generated by taking account of physical laws that govern the monitored power system. Traditionally, ground controllers utilize the second level of redundancy in that they compare any sus-

picious sensor measurements against probable measurements, which, heretofore, they have calculated by hand.

Although NASA has employed autonomous electrical power systems for several years, computers have not been used to help ground controllers diagnose anomalies in sensor measurements. Control-center consoles have merely alerted controllers when sensor readings have exceeded set maximum or fallen below set minimum values.

The present algorithm systematically filters possibly conflicting and erroneous sensor data to determine the most probable values of critical measurements. The algorithm generates the most probable values of current and voltage for the sensors in question, draws conclusions from statistical information, and indicates, to ground controllers, one of three possible types of causes for any anomalies: sensor failures, soft faults, and sensor drift.

The algorithm, implemented in a C++ computer program, calculates the most probable values from all available measurements, real and calculated. If a value does not fall within the 3-standard-deviation (3 σ) range for all measurements, the measurement that differs most from the estimated value is eliminated from the calculation. This procedure is repeated until either the estimate falls within the 3 σ range for the remaining measurements or only two disagreeing measurements are left, in which case the value is considered indeterminate. The most probable values of sensor measurements are calculated from the means and variances of redundant values, creating a weighted average based on the variance of each sensor.

This work was done by Wallace Kelly III of Rockwell Space Operations Company for Johnson Space Center. Further information is contained in a TSP [see page 1], MSC-22728

Automated Apparatus for Testing Gyroscopes

Except for initial setting of conditions, the entire testing process is automated.

NASA's Jet Propulsion Laboratory,
Pasadena, California

The Gyroscope Automated Testbed is a computer-controlled apparatus designed primarily for automated testing of vibratory gyroscopes. It can also be used to test other devices. By changing testing-system-tested-device interface circuitry that is part of the apparatus, one can set up the apparatus to test nonvibratory gyroscopes. The apparatus can also be used as a general-purpose noise-analysis system for characterizing a variety of devices in addition to gyroscopes.

Heretofore, it has been necessary to resort to a manual process to test gyroscopes. The process is very time-consuming and requires expensive test equipment. The present apparatus automates most of the process for a fraction of the cost.

The apparatus (see Figure 1) is based on a Pentium II computer with a 16-bit data-acquisition card and a GPIB (general-purpose interface bus) interface cord. Custom software for control of testing and analysis of data has been developed in Visual Basic. The system is fully automated and only requires an operator to initially set the desired testing conditions. The software can perform a rotational-response test, noise

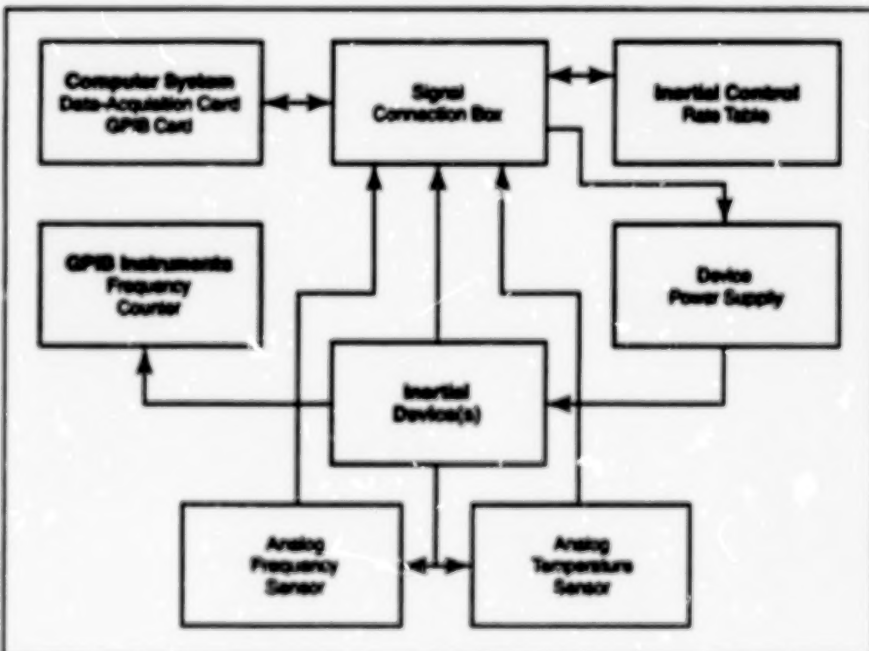


Figure 1. This Simplified System Diagram depicts the major functional blocks of the Gyroscope Automated Testbed.

characterization test, and a power-cycle stability test. Data analysis is performed on the acquired data to characterize the rotational

response and power-cycle stability (see Figure 2). A Green chart and a plot of the power spectral density (PSD) are generated

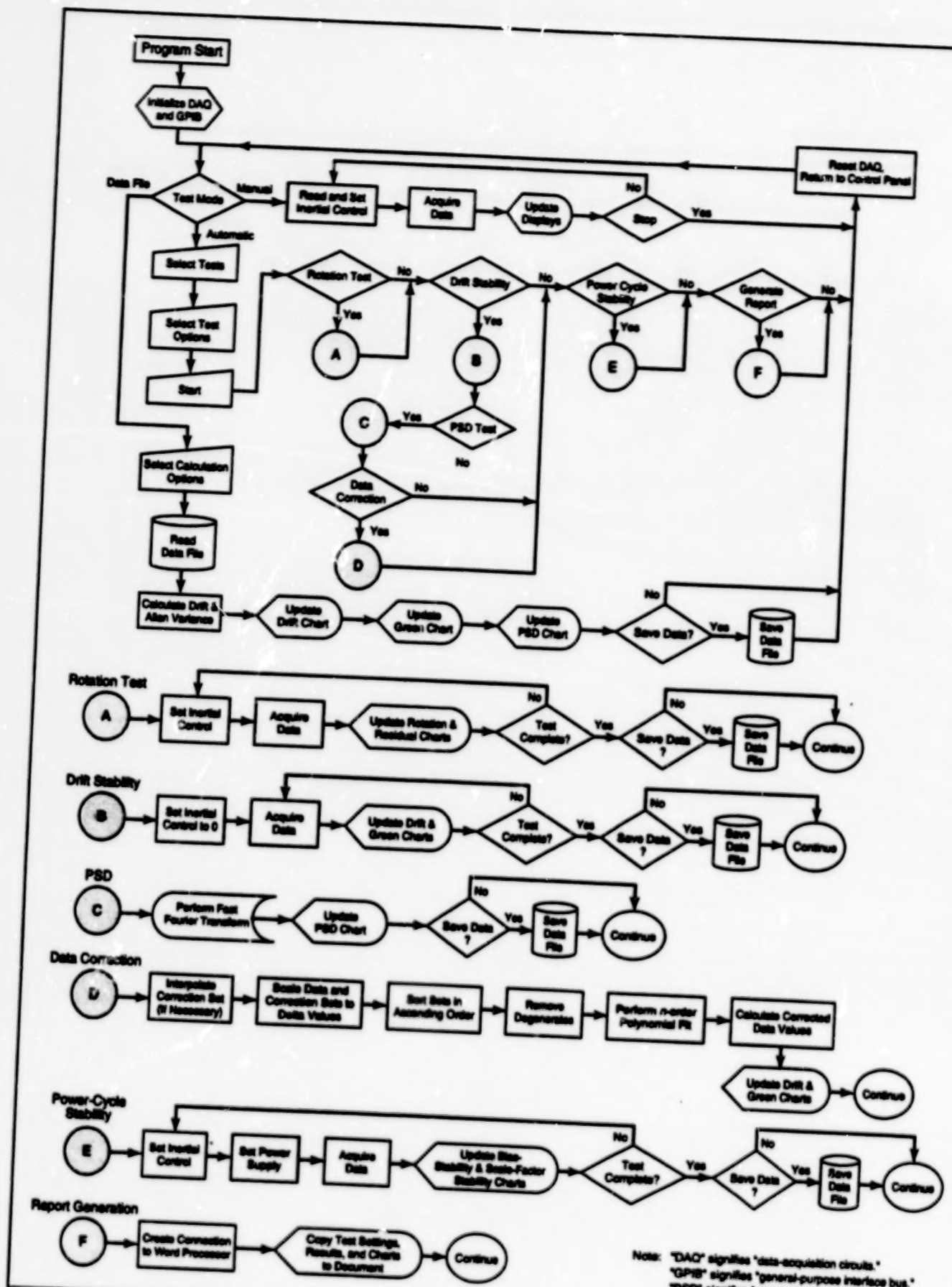


Figure 2. This Flow Chart represents the automated test procedure implemented by the custom software in the Gyroscope Automated Testbed.

to characterize the noise properties of the device being tested. Device drift and Green charts can be corrected (linearized) by any other sampled data set (i.e., the drift data can be corrected for increasing temperature over the duration of a test). A report, which consolidates the results into a convenient document, is generated automatically upon

completion of all tests. The software includes provisions for selecting the tests to be performed, setting test parameters, saving acquired data to a file, generating real-time output displays, testing under manual control, and deriving noise characteristics from previously acquired data.

This work was done by Christopher

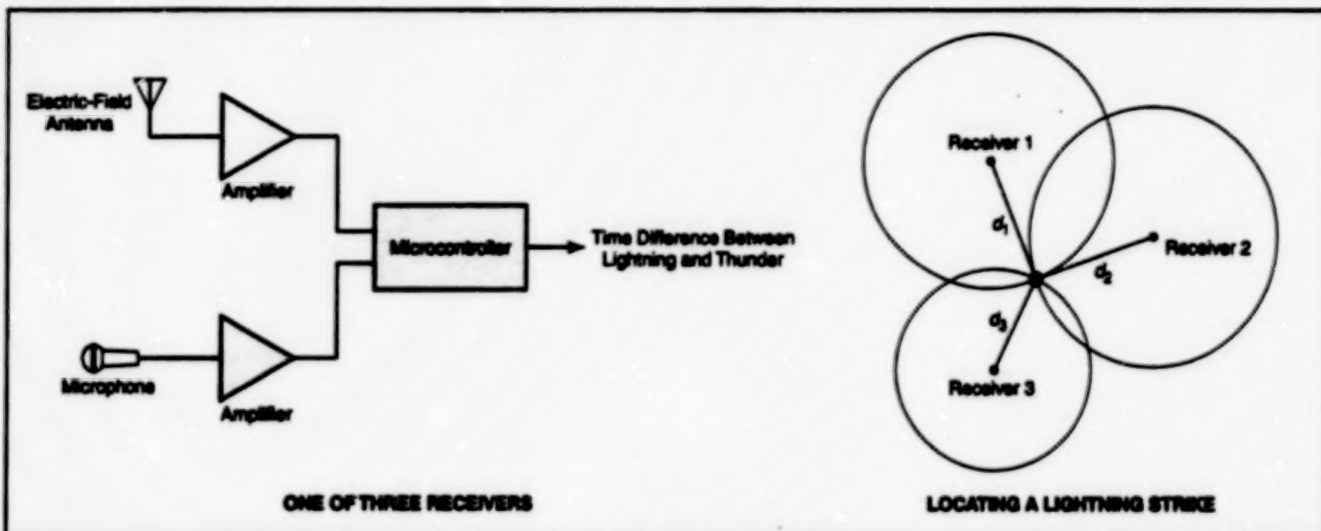
Evans and Roman Gutierrez of Caltech for NASA's Jet Propulsion Laboratory. Further information is contained in a TSP [see page 1].

This software is available for commercial licensing. Please contact Don Hart of the California Institute of Technology at (818) 393-3425. Refer to NPO-20612.

System Locates Lightning Strikes to Within Meters

Locations are determined from propagation times for electric and sonic fields.

*John F. Kennedy Space Center,
Florida*



The Distances of Three Receivers from a lightning strike is computed from the speed of sound and the times for propagation of thunder to the receivers. The location of the strike is identified as the intersection of radii equal to these distances.

A system for determining the locations of nearby lightning strikes from electric-field and acoustic measurements has been developed and built. The system includes at least three receivers, each equipped with an antenna and a microphone. For each strike, the system measures the difference between the times of arrival of the electric-field and sonic (thunder) pulses at each receiver, computes the distance of the strike from the time difference and the speed of sound (about 320 m/s), then uses the distances to determine the location of the strike. The basic concept of this system is thus a variant and extension of the time-honored concept of estimating the distance of a lightning strike from the difference between the times of arrival of the visible flash and the audible thunder.

"Nearby" as used here signifies that the receivers and the lightning strikes of interest are located at distances of the order of 1 km from each other. Older lightning-location systems cover observation areas with radii of the order of 30 miles (48 km), and typically locate lightning strikes with errors of the order of 0.5 km or more; thus, the older systems do not locate strikes accurately enough for purposes of

assessing actual or potential damage by lightning to specific structures and pieces of equipment. The developmental system locates strikes to within errors of the order of a meter.

Unlike in some other systems, there is no need for expensive, high-speed waveform digitizers. Instead, the leading edge of the electric-field pulse detected in each receiver is used to start a timer, and the leading edge of the thunder pulse arriving at the same receiver is used to stop the timer. A microcontroller in each receiver transmits the time thus measured to a processing station, where the times are converted to distances that are used to compute the location of the lightning strike (see figure).

The accuracies achievable by older systems and by this system can be compared via consideration of the time-measurement problem. Given that the applicable speed in this system is the speed of sound, even a timing error as large as 1 ms in this system would result in a distance error of only about 0.3 m. However, in a typical older system based on the speed of light, the allowable timing error to achieve such accuracy in distance would be only about 1 ns.

Thus far, only one receiver has been

tested. It has been shown to be capable of measuring the distances to lightning strikes. Optionally, the fully developed system could contain more than the minimum of three receivers needed to determine the location of a lightning strike unambiguously under ideal conditions. The additional receivers could be used to enhance accuracy under nonideal conditions. By use of a suitable algorithm, the partly redundant data from more than three receivers could be used to resolve uncertainties introduced by wind and by echoes from nearby objects. The wind problem is especially important because in the presence of wind, the equal propagation-time distance contour around each receiver becomes distorted from a circle.

This work was done by Pedro J. Medallus formerly of I-NET, Inc., for Kennedy Space Center. Further information is contained in a TSP [see page 1].

Inquiries concerning rights for the commercial use of this invention should be addressed to the Technology Programs and Commercialization Office, Kennedy Space Center, (407) 867-6373. Refer to KSC-11992.

Portable ECG/EGG Data Recorder

This is a noninvasive unit that interferes minimally with normal activities.

Lyndon B. Johnson Space Center,
Houston, Texas

A portable electronic unit with no moving parts except button switches digitizes and stores a 48-hour record of the myoelectric activity of the stomach and heart as sensed via electrodes on the surface of the abdomen. Just as the more familiar electrocardiogram (ECG) is useful in diagnosing the condition of the heart, the digital electrogastrogram (EGG) that is also obtained by this portable data recorder is useful in assessing changes in gastric function.

This unit, called the "BioLog," was originally designed to aid studies of gastric changes and related changes in the activity of the autonomic nervous system associated with space motion sickness in astronauts. However the unit can also be used on Earth to collect the same or other types of physiological data from patients who object to the restrictions imposed by traditional stationary physiological monitoring equipment. The unit has a volume of < 1,000 cm³ and a mass of 0.68 kg. It can be mounted on the wearer's belt or attached to the wearer's clothing by use of hook-and-pile fastening material and a custom-designed pocket.

The unit is connected to high-input-impedance, low-output-impedance amplifiers that, in turn, are connected directly (via snap-on fasteners) to the electrodes on the patient's abdomen. This arrangement provides sufficient amplification at the signal source and sufficient immunity to extraneous electrical noise that the signal-to-noise ratio is great enough for ambulatory recording, unlike in older EGG recorders in which ambulatory recording was rendered useless by motion-induced artifacts in the signal.

The EGG can be discerned as a shift in the baseline of the ECG because the characteristic frequencies of the ECG (typically > 1 Hz) are significantly greater than those of the EGG (typically = 0.05 Hz). The unit

digitizes and records the ECG/EGG at a sampling rate of 10 Hz. When the recorded data are subsequently analyzed, they are filtered to separate them into EGG and ECG components.

The unit includes a clock that generates time tags for the data. A 9-V alkaline battery supplies the main operating power. When the main power is off, a capacitor of about 1 farad supplies backup power to keep the clock running for 29 days. A 16-character liquid-crystal device (LCD) displays the current time (in days, hours, and minutes) or other information as needed.

The data-storage medium is a static random-access memory (SRAM) circuit card. The SRAM is structured to enable the recording, within the single data channel, of event markers and other ancillary information time-locked to the ECG/EGG data. The recording of ancillary data involves the insertion of alternate data structures in the data stream. Two types of activity and the associated alternate data structures are accommodated; those that involve suspension of data logging and those for which the data recorded before and after are contiguous in time.

Activities that involve suspension of data logging include turning power on or off, resetting the clock, resetting recording to the beginning of the SRAM (this erases all data recorded previously), and calculation of system resources (battery power and the remaining unused portion of the SRAM). Activities that do not involve suspension of logging include the insertion of event markers by pressing of button switches on the outside of the unit. Five button switches and corresponding event markers are available and can be defined as the user sees fit, without modification of hardware or software. An alternate data structure identifies which event-marker

button has been pressed and causes the report of the event to be time-locked to the data that follow. At the moment when an alternate data structure is inserted, the ECG/EGG data are stored in a buffer so that no discontinuity in the data occurs. To prevent activation by accidental contact, an event marker is not inserted until the corresponding button switch has been pressed for 1 second. When the data are subsequently analyzed, the alternate data structures are removed and, in cases of no interruption in logging, the data from before and after are concatenated.

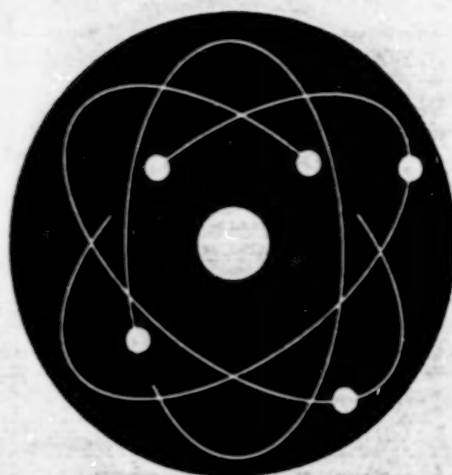
An error code is displayed on the LCD to alert the user to problems with the operation of the unit. There are four error codes; the first indicates that the battery charge is too low, the second indicates that the SRAM card is inserted improperly, the third states the SRAM card is write-protected, and the fourth indicates that the SRAM was not properly initialized. The occurrence of any of these conditions prevents operation.

This work was done by Deborah L. Herm of Johnson Space Center, Gwenn R. Sandoz and Charlene R. Jacobsen of KRUG Life Sciences, and Harve M. Harish and Marty Loughry of UFI, Morro Bay, CA. Further information is contained in a TSP [see page 1].

In accordance with Public Law 96-517, the contractor has elected to retain title to this invention. Inquiries concerning rights for its commercial use should be addressed to

KRUG Life Sciences, Inc.
1290 Hercules, Suite 120
Houston, TX 77058

Refer to MSC-22677, volume and number of this NASA Tech Briefs issue, and the page number.



Physical Sciences

Hardware, Techniques, and Processes

- 19 Soaring to 100,000 ft on Stratospheric Mountain Waves
- 20 Ultrasonics With Laser In-Coupling and Air Out-Coupling
- 21 Designing Purging Flows of Clean, Dry Gases
- 22 Sulfur Lamp With CaBr_2 Additive for Enhanced Plant Growth
- 23 Measuring NO and OH Concentrations at High Pressure

Books and Reports

- 23 Simulations of Evolving Transitional Mixing Layers
- 24 Simulations of a Transitional Droplet-Laden Mixing Layer
- 24 Thermodynamic Instability of $\text{In}_x\text{Ga}_{1-x}\text{As}$ /GaAs Quantum Dots

18

BLANK PAGE

Soaring to 100,000 ft on Stratospheric Mountain Waves

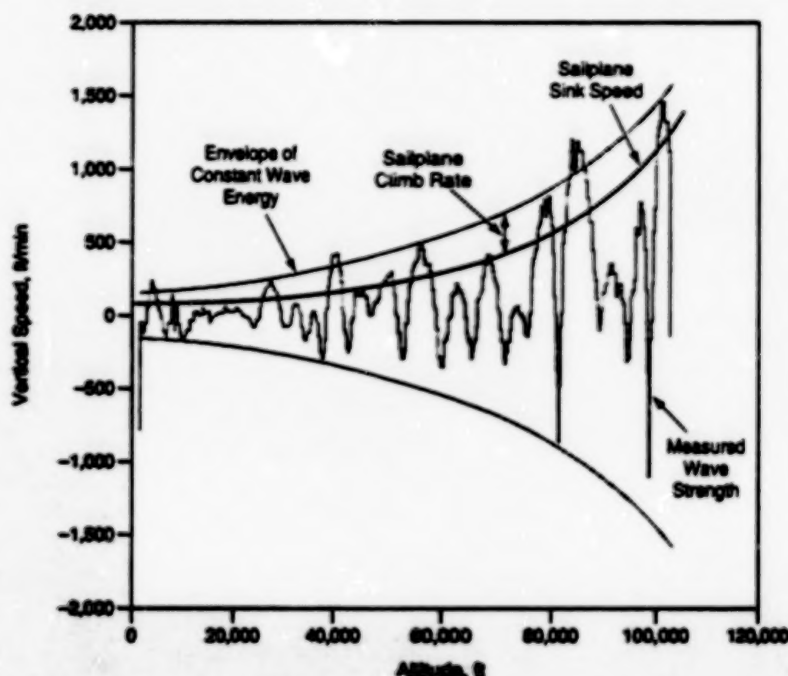
A proposed sailplane would make the most of these waves.

Dryden Flight Research Center,
Edwards, California

A research project now underway addresses the concept of utilizing stratospheric mountain waves to soar to high altitudes in sailplanes. Stratospheric mountain waves are mountain waves that propagate strongly, and with continuity, into the middle and upper stratosphere, and are not extinguished, trapped, or reflected at or near the tropopause. The historical experience of high-flying aircraft has been limited to the lower region of their domain, where large amplification leading to large vertical speeds and instability is uncommon. Amplification with increasing altitude, and the instability caused by this amplification, can lead to wave overturning, similar to waves breaking at the beach. Wave overturning originating from amplification has not been experienced by aircraft yet, as far as we know. The general impression of the stratosphere as an entirely quiet region is not, in general, justified.

Recently, high-altitude meteorological research balloons, launched in support of other atmospheric-science projects, have recorded very strong mountain waves (see figure) up to a balloon-burst altitude of 105,000 ft (32 km). The waves propagate into the middle or upper stratosphere when the outer region of the polar vortex lies above a strong tropospheric wind band, above mountainous terrain. In this situation, there is no appreciable wind maximum at the tropopause, and little evidence of a tropopause in the temperature profile. Waves propagate upward with increasing vertical wind component. Stratospheric mountain waves are most commonly found, in the Northern Hemisphere, in the 60°-to-70° latitude band. In the Southern Hemisphere, they extend further toward the equator, because of the larger extent of the polar vortex in that hemisphere. Stratospheric waves can also form (albeit very rarely) at lower latitudes.

The present project is the first step to build and demonstrate the utility of a special-purpose piloted research sailplane that can climb in strong stratospheric mountain waves to its lift-limited ceiling. For a sailplane with state-of-the-art structural and aerodynamic characteristics, the lift-limited ceiling lies between 100,000 and 110,000 ft (30.5 and 33.5 km). Flights are to be made safely and repeatedly, as justified by the need for experimental data.



Mountain-Wave Vertical Speeds are plotted alongside the sailplane sink rate and the corresponding estimated sailplane climb rate.

Work to gather additional data on the strength, location, structure, and frequency of occurrence of strong mountain waves is now underway. The data are expected to verify that the aerodynamic performance of a sailplane will enable it to climb to 100,000 ft (30.5 km) in the waves. In addition, simulations are expected to determine what degree, if any, of stability augmentation will be necessary for the sailplane.

The meteorological part of the work will consist of identification and searching of historical sources of mountain-wave data. In addition to searching such pre-existing data, special dedicated balloon ascents with Global Positioning System (GPS) sondes will be made to augment the data normally obtained from sondes launched at regular intervals and from other special balloons that are used for research not related to stratospheric mountain waves. The meteorological profile characteristics will be summarized with respect to the characteristics of waves identified in the balloon data. Numerical modeling of mountain waves will be done for selected cases found in the data acquired from the

sondes during the dedicated balloon ascents and from other sources.

The work will include an aerodynamic-performance part based on a standard "drag build up" method. This part of the work will involve the use of pre-existing basic data sources and of incremental variations on pre-existing high-performance sailplanes for which accurate performance measurements have been made.

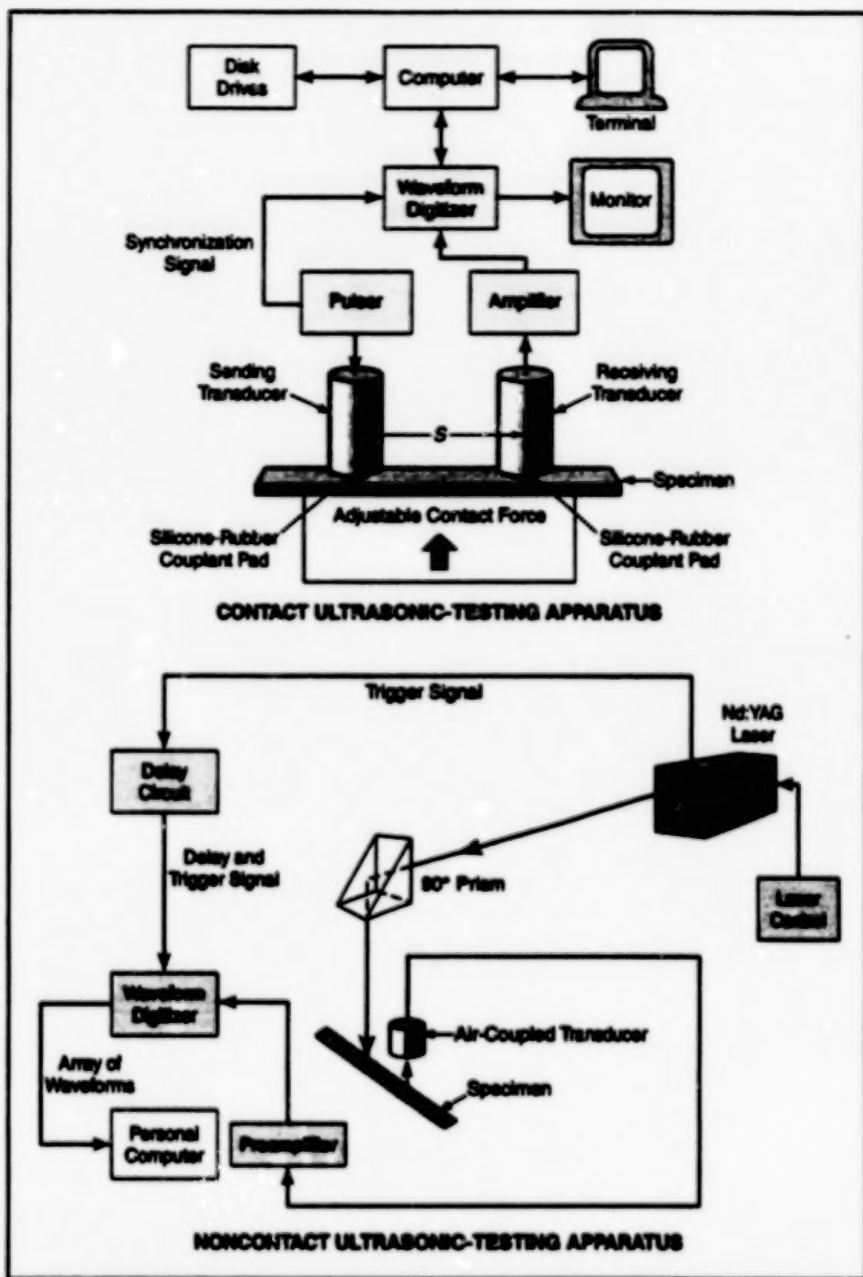
The simulation part of the work will include assessment of the flying qualities of the sailplane. With the Dryden simulation, actual or numerical models of the wave structure can be included. The direct effect of the wave structure on sailplane control can be shown. The effect of turbulence generated in wave overturning events will not be as realistically modeled. Variations of parameters will be made to determine the most attractive combination of aerodynamic stability and augmentation.

This work is being done by Edward H. Teets, Jr., of Dryden Flight Research Center and by Einar Enevoldson of Norjen, Inc., under a Flight Test Technique grant and a Dryden Discretionary Fund grant. DRC-00-08

Ultrasonics With Laser In-Coupling and Air Out-Coupling

This method shows promise for noncontact, nondestructive characterization of materials and structures.

John H. Glenn Research Center,
Cleveland, Ohio



The Noncontact Ultrasonic-Testing Apparatus with laser in-coupling and output coupling via air reproduces the basic geometry of the contact apparatus.

Efforts are under way to develop a technique of noncontact acousto-ultrasonic testing in which (1) a pulsed laser beam excites ultrasonic waves in a plate specimen and (2) the ultrasonic waves are detected by use of one or more focusing air-coupled ultrasonic transducer(s) placed at a short distance away from the specimen and aimed at the spot(s) of interest on the specimen. This technique is intended to be an

alternative to an older technique of contact acousto-ultrasonic testing; when fully developed, this noncontact technique could be used to characterize materials and monitor integrity of structures in locations that are inaccessible to contact ultrasonic probes or in situations in which contact ultrasonic probes cannot or should not be used.

The acousto-ultrasonic method has been shown to be useful for assessing

mechanical properties of composite-material structures. Plate-wave analysis has been used to quantify moduli of elasticity of composite materials. Rates of decay of ultrasonic signals can be used to monitor residual strengths or crack densities. The present development is expected to extend these capabilities from the contact to the noncontact regime. It has been envisioned that noncontact acousto-ultrasonic testing technique would be especially useful for monitoring changes in the properties of ceramic- and metal-matrix composite materials, and of aircraft-engine structural components made of these materials, during thermomechanical testing and during engine operation.

The use of a laser as a remote (and thus also noncontact) ultrasound-input source and as part of an ultrasound detector has been under investigation for a number of years. The use of a noncontact piezoelectric ultrasonic transducer coupled through an airgap has also been under study. Laboratory experience has led to the conclusion that a laser is more useful as an ultrasound-input device than as part of a detector, while an air-coupled piezoelectric transducer is more useful as a detector than as an ultrasound-input device. Taking advantage of this lesson of experience, the present laser-in-coupling/air-out-coupling technique combines the two named means of coupling in a way as to obtain a signal-to-noise ratio greater than can be achieved in other noncontact ultrasonic techniques that involve laser or air coupling.

The figure schematically depicts two acousto-ultrasonic testing apparatuses; one that implements an older contact technique and one that implements the present noncontact technique. In the noncontact apparatus, the beam from a pulsed neodymium: yttrium aluminum garnet (Nd:YAG) laser is aimed at a spot on the specimen; this is the same spot where, in the contact apparatus, the sending transducer would be coupled to the specimen via a dry (silicone rubber) couplant pad. The air-coupled transducer in the noncontact apparatus is positioned and oriented to be sensitive to the spot on the specimen where, in the contact apparatus, the receiving transducer would be coupled to the specimen via another silicone rubber pad. A nonfocusing microma-

chined capacitance transducer can be used as an alternative to the air-coupled piezoelectric transducer (and is characterized by a broader frequency response), provided that it can be placed close enough to the specimen.

In experiments, rates of decay of ultrasonic energy in SiC/SiC ceramic-matrix and SiC/Ti metal-matrix composite-material specimens were measured by the contact technique and by the present noncontact technique. For each noncontact measurement, the laser pulse energy was ≈ 13 mJ and the air-coupled acoustic transducer was one with a broad frequency response nominally centered at 0.25, 0.5, 1.0, or 2.0 MHz. The rates of decay of ultrasonic energy were found to be higher

for the contact measurements; the difference has been attributed to loss of energy via the contacts, and this attribution, in turn, seems to imply that the noncontact rate of decay is a more nearly pure measure of attenuation of ultrasound within the specimen. Still, contact measurements have been successful in revealing mechanical fatigue in the specimen materials; it is important that this be so, inasmuch as in projected uses for monitoring the integrity of aircraft components, it will often be necessary to take measurements in the presence of support structures that cause loss of ultrasonic energy. In both the contact and noncontact techniques, rates of decay of ultrasonic signals have been observed to increase with frequency.

Several concerns must be addressed in further development efforts. One is potential destructiveness of the laser pulse. Another is attenuation of the ultrasonic signal in output coupling via air; this attenuation imposes a practical upper limit on the useable frequency range.

This work was done by Harold E. Kautz of **Glenn Research Center**. Further information is contained in a TSP [see page 1].

Inquiries concerning rights for the commercial use of this invention should be addressed to NASA Glenn Research Center, Commercial Technology Office, Attn: Steve Fedor, Mail Stop 4-8, 21000 Brookpark Road, Cleveland, Ohio 44135. Refer to LEW-18916.

Designing Purging Flows of Clean, Dry Gases

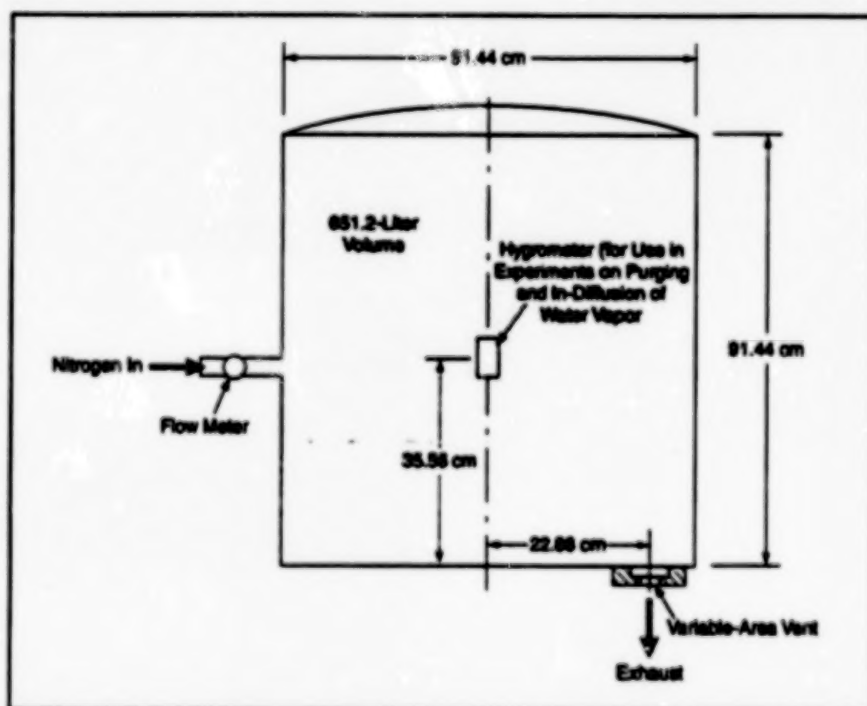
Flow parameters can be chosen to reduce contamination to specified low levels.

*Goddard Space Flight Center,
Greenbelt, Maryland*

A method of designing purging flows of clean, dry gases to maintain acceptably low levels of contamination in enclosed volumes has been developed. The method is applicable to diverse enclosures that must be kept clean, including housings of precise optical instruments, clinical facilities, facilities for manufacturing microelectronic devices, and clean rooms in general.

In the simplest case, the purging flow of clean, dry gas is required to limit the entrance of external contaminants into the purged volume through a single purge vent (see figure). External contaminants include gases (e.g., water vapor) and particles (e.g., microbes and dust). Also, typically, the purging flow is required to limit the concentration of contaminants generated internally by outgassing and to sweep out these contaminants. The present design method, based on equations developed in a theoretical and experimental study of bulk and diffusional flow, enables one to select the pressure, flow speed, and volumetric flow rate of the purge gas to satisfy these requirements.

The purging volumetric flow rate needed to limit potentially contaminating external air to an acceptably low partial pressure is a function of its partial pressure, of the ambient pressure, and of the characteristic time for entry of air or of the contaminant(s) of interest into the volume through the purge vent. This characteristic time can be determined experimentally. The purge-gas pressure needed to maintain the required



A Tank Purged With Nitrogen through a single inlet and a single outlet was used in experiments to obtain parameters for purge-flow design equations.

volumetric flow through the purge vent can be calculated as a function of the ambient temperature and pressure and the cross-sectional area of the purge vent. The speed of flow through the vent is, of course, directly related to the volumetric flow rate and the cross-sectional area of the vent. The size of the largest airborne particle that can be prevented from entering against the

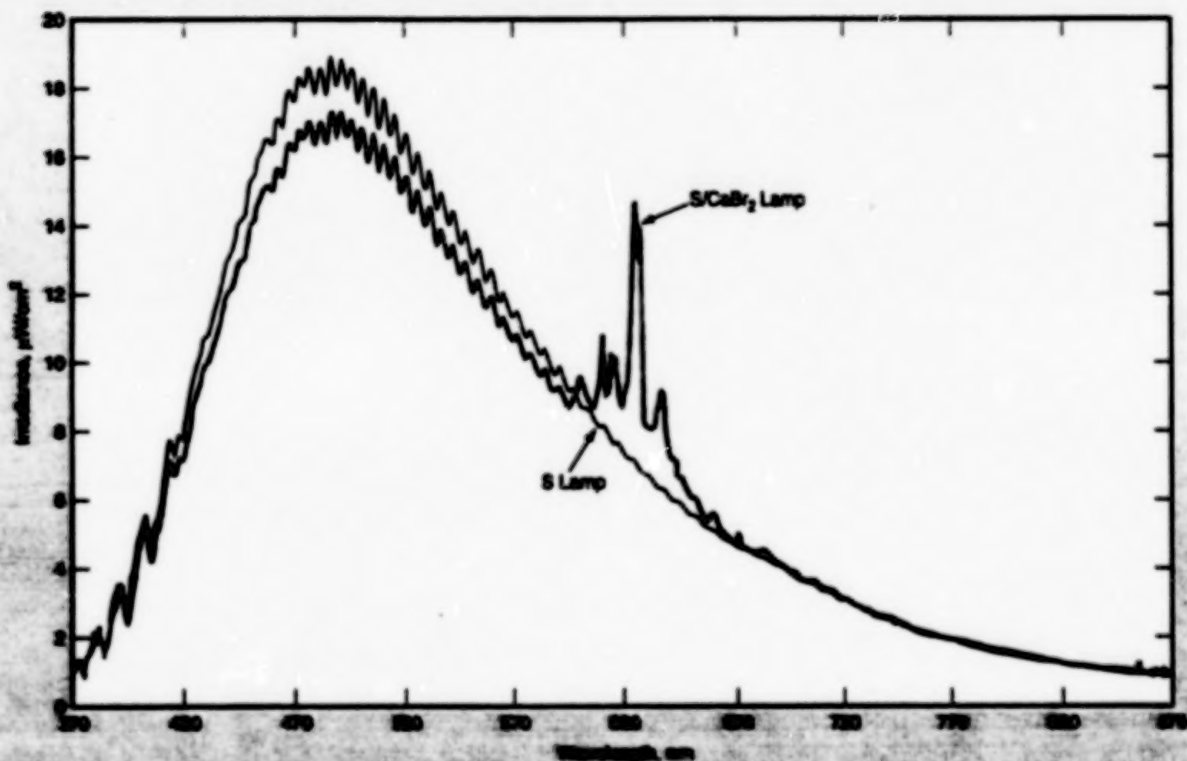
purging flow can be calculated as a function of the flow speed and of the viscosity and mass density of the vented gas.

This work was done by John J. Scialdone of **Goddard Space Flight Center**. Further information is contained in a TSP [see page 1].
GSC-14241

Sulfur Lamp With CaBr_2 Additive for Enhanced Plant Growth

Addition of CaBr_2 intensifies red light, which is favored by plants.

John F. Kennedy Space Center,
Florida



The Measured Spectrum of A Sulfur/Calcium Bromide Lamp is plotted along with the spectrum of a similar sulfur lamp without calcium bromide. The prominent spectral peak of the S/CaBr_2 lamp lies at the wavelength region of highest quantum efficiency for photosynthesis in plants.

Calcium bromide can be added to the sulfur filling in a sulfur lamp to increase the emission of red light for enhanced growth of plants. Red light is more efficacious for plant growth than is visible light at shorter wavelengths. The addition of CaBr_2 increases the emission at wavelengths in the vicinity of 625 nm, where the quantum efficiency for photosynthesis is close to 1.

A sulfur lamp is an electrodeless lamp that includes an evacuated quartz bulb partly backfilled with argon and with a little sulfur, plus a source of microwave power for exciting a plasma within the bulb. A sulfur lamp is very efficient for visible lighting. An attempt to increase the emission of red light by increasing the sulfur content would result in an excessive reduction in the emission of blue light. Alternatively, following a common practice in the lighting industry,

one could attempt to increase the red emission by adding such metal halides as sodium iodide; in the presence of the lamp plasma, the metal atoms in most such additives become excited and ionized and they radiate in the desired spectral region, but they also emit unwanted infrared line radiation, with a consequent reduction in efficacy for growth of plants.

Unlike other metal halide additives, in the presence of the lamp plasma, calcium bromide emits primarily molecular radiation at wavelengths in the vicinity of 625 nm, with minimal infrared emission. Thus, calcium bromide can be used to increase the emission of the desired red light. A representative experimental lamp based on this concept is made of a thin-wall, 35-mm-diameter quartz bulb containing tens of milligrams of sulfur, a few milligrams of CaBr_2 , and argon at a pressure of about 50 torr

(6.7 kPa). As shown in the figure, the CaBr_2 filling increases the desired red emission at the cost of only a small decrease in shorter-wavelength emission and with little or no increase in infrared emission.

This work was done by Youngzhong Leng and Donald A. MacLennan of Fusion Lighting, Inc., for Kennedy Space Center.

In accordance with Public Law 96-517, the contractor has elected to retain title to this invention. Inquiries concerning rights for its commercial use should be addressed to

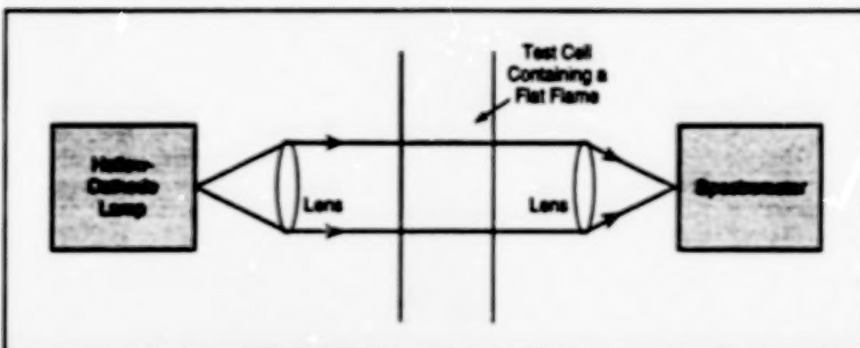
Donald A. MacLennan
Fusion Lighting
7524 Standish Place
Rockville, MD 20855
(301) 284-7200

Refer to KSC-11970, volume and number of this NASA Tech Briefs issue, and the page number.

Measuring NO and OH Concentrations at High Pressure

An optoelectronic laboratory apparatus could be developed into a portable instrument.

John H. Glenn Research Center,
Cleveland, Ohio



Ultraviolet Light that resonates with absorption spectral lines of a gas species of interest is directed through the test cell. The spectrum of transmitted light is measured and processed to determine the concentration of the species of interest in the test cell.

An apparatus based on line-of-sight resonant absorption of ultraviolet light yields measurement data from which one can calculate the concentrations of nitric oxide (NO) and of hydroxyl radicals (OH) in a laboratory flat flame at a pressure up to 30 atm (≈ 3 MPa). The basic measurement principle is distinct from the principles of laser-induced fluorescence and other laser diagnostic techniques; hence, the data generated by this apparatus could provide independent verification of data from laser-based instruments.

Line-of-sight resonant absorption of ultraviolet light has been in use at least since 1976; however, until now, it had not been experimentally verified to be useful for determining NO and OH concentrations at pressures above 2 atm (≈ 0.2 MPa). The high-pressure-flame regime of the present development was chosen because it is representative of conditions at the exit of advanced combustors. The design of the apparatus and the measurement principle are simple enough that it should be possible to develop the apparatus into a portable optoelectronic instrument that could be set up in combustor or engine test cells.

In the apparatus (see figure) a water-cooled hollow-cathode lamp generates ultraviolet light, which is collimated and directed through a test cell that contains the flame to be probed. The portion of the collimated beam that remains after pass-

ing through the test cell then enters a fiber-optic cable, through which it travels to the entrance slit of a computer-controlled grating spectrometer equipped with a linear array of 1,024 photodiodes at its output plane. The spectrometer measures the spectrum of light that has passed through the test cell, at wavelengths from 208 to 280 nm (for NO) or 300 to 330 nm (for OH) with a spectral resolution of 0.3 nm.

For measuring the concentration of NO, a glow discharge in flowing air at a pressure of 5 to 10 torr (≈ 0.7 to 1.3 kPa) is created in the hollow-cathode lamp. The light from this discharge includes discrete emission spectral lines generated by the recombination of O and N with N_2 and O_2 . Thus, the emitted light includes components that resonate with the absorbing species of interest. Although one could use a continuum light source (at least in principle), resonant absorption offers the advantage of a greater signal-to-noise ratio. For measuring the concentration of OH, the lamp is operated in a similar manner except that the glow discharge is created in an atmosphere of argon saturated with water.

The spectrum of transmitted light is well approximated by a mathematical model of transmissivity as a function of wavelength, the temperature of the flame, the length of the optical path through the flame, and the concentration and optical-absorption characteristics of the gas species (NO or

OH) of interest. The model was developed to nearly its present form in 1980 and was refined, for use in the present application, by incorporating terms to account for shifting and pressure broadening of spectral lines of both NO and OH.

In use, an assumed value of the concentration of the species of interest is inserted in the model of transmissivity along with the known values of the other quantities and the model is convolved with a spectrometer-slit function to obtain a predicted spectrometer output. This computation is repeated, if necessary, using different values of assumed concentration. The concentration of the species of interest is then deemed to equal whichever value of assumed concentration results in the best match between the predicted and actual spectrometer outputs.

In tests, the apparatus was used to measure spectra during operation of the cell with flames at two different fuel/air mixture ratios (fuel concentrations of 0.98x and 1.3x stoichiometric) and at several pressures from 1 to 30 atm (≈ 0.1 to 3 MPa). Concentrations of NO and OH were measured independently by a conventional gas-sampling technique. The absorption spectra measured by the apparatus agreed, within 25 percent, with absorption spectra predicted by the mathematical model. Continuum absorption in hot oxygen was found not to be strong enough to interfere significantly in interpretation of the data on absorption in NO.

This work was done by D. S. Lischinsky, B. A. Knight, and J. A. Shirley of United Technologies Research Center for Glenn Research Center. Further information is contained in a TSP [see page 1].

Inquiries concerning rights for the commercial use of this invention should be addressed to NASA Glenn Research Center, Commercial Technology Office, Attn: Steve Fedor, Mail Stop 4-8, 21000 Brookpark Road, Cleveland, Ohio 44135. Refer to LEW-16914.

Books and Reports

Simulations of Evolving Transitional Mixing Layers

A report describes direct numerical simulations of single- and two-phase, tempo-

rally developing transitional mixing layers at Reynolds numbers (based on the initial vorticity thickness and mean velocity difference) from 200 to 600. As many as $300 \times 332 \times 180$ grid points were used to dis-

cretize the gas phase. As many as 5.7×10^6 individual evaporating droplets of various sizes, present in liquid-to-gas mass ratios between 0 and 0.5, were tracked in a Lagrangian reference frame. The gas

phase was described by the Navier-Stokes equations for a compressible fluid, augmented by species-transport equations and by the energy equation. In the conservation equations, source terms account for the coupling of mass, momentum, and energy between phases. The equations were solved by eighth-order-accurate central finite spatial differencing, together with fourth-order explicit Runge-Kutta time integration. The numerical results capture the mixing transition to small-scale turbulence with momentum-thickness Reynolds numbers as large as $\approx 1,400$ during a second pairing of spanwise vortices. There are discussions of the evolution of the transition to turbulence and of efficient parallel computer coding of the mixed Eulerian/Lagrangian flow problem.

This work was done by Josette Beilan and Richard Miller of Caltech for NASA's Jet Propulsion Laboratory. To obtain a copy of the report, "Evolution of Single-Phase and Droplet Laden Transitional Mixing Layers," see TSP's [page 1]. NPO-207115

Simulations of a Transitional Droplet-Laden Mixing Layer

A report describes direct numerical simulations of a droplet-laden mixing layer (e.g., evaporating droplets of a hydrocarbon fuel in air) undergoing a transition to mixing turbulence. The governing equations are those of Lagrangian transport of discrete droplets through a flowing gas, which is represented by Eulerian equations

with source terms for two-way couplings of mass, momentum, and energy among the liquid, vapor, and carrier-gas phases. The equations are solved numerically, using as many as 18×10^6 grid points to discretize the Eulerian gas-phase equations and tracking as many as 5.7×10^6 evaporating droplets of various initial sizes in the Lagrangian reference frame. At large Reynolds numbers, the numerical solutions capture the complete transition to mixing turbulence. It is observed that increasing the droplet mass-loading ratio results in a more "natural" turbulence characterized by more rotational energy and less influence of initial forcing perturbations, along with increased droplet organization within the layer. The numerical solutions are utilized as a data base in several analyses of the errors introduced into large-eddy simulations by ignoring subgrid fluctuations of velocities and thermodynamic quantities.

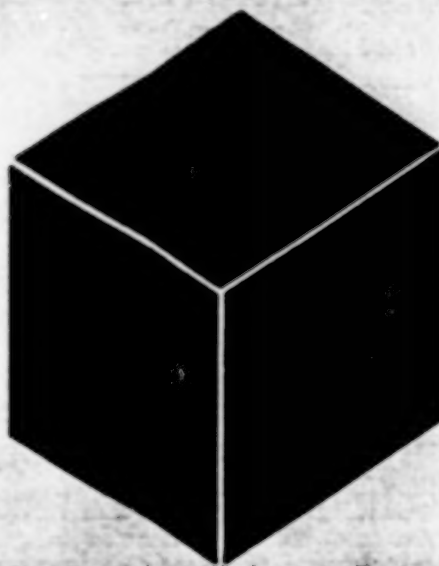
This work was done by Josette Beilan and Richard Miller of Caltech for NASA's Jet Propulsion Laboratory. To obtain a copy of the report, "Direct numerical simulation and subgrid analysis of a transitional droplet laden mixing layer," see TSP's [page 1]. NPO-20709

Thermodynamic Instability of $\text{In}_{x}\text{Ga}_{1-x}\text{As}/\text{GaAs}$ Quantum Dots

A report describes experiments that generate evidence of thermodynamic instability of nanometer-size islands (quantum dots) in $\text{In}_{x}\text{Ga}_{1-x}\text{As}$ grown on GaAs.

$\text{In}_{x}\text{Ga}_{1-x}\text{As}/\text{GaAs}$ specimens were grown by metal-organic chemical vapor deposition, using various partial pressures of AsH_3 . Examination of specimens by force microscopy, electron microscopy, and low-temperature photoluminescence spectroscopy revealed differences in island formation at different partial pressures of AsH_3 , including differences in (1) surface coverages of islands, (2) ratios between numbers of coherent and incoherent islands, (3) sizes and shapes of islands after annealing, and (4) thicknesses for the onset of the Stranski-Krastanow (S-K) transformation (in which quantum dots form spontaneously in a second semiconductor deposited on a lattice-mismatched first semiconductor once the second semiconductor reaches a critical thickness, which is typically a few molecular layers). The differences showed that increasing the partial pressure of AsH_3 reduces the surface coverage of islands and delays the onset of the S-K transformation to greater thickness. It was also found that small, thermodynamically stable, unfaceted, lens-shaped islands can form if $\text{In}_{x}\text{Ga}_{1-x}\text{As}$ surface energies are minimized. These findings lead to the conclusion that at sufficiently high concentration, AsH_3 can raise surface energies, thus acting as an impurity-free surfactant.

This work was done by Rose Leon of Caltech for NASA's Jet Propulsion Laboratory. To obtain a copy of the report, "Island Shape Instabilities and Surfactant-Like Effects in the Growth of $\text{In}_{x}\text{Ga}_{1-x}\text{As}/\text{GaAs}$ Quantum Dots," see TSP's [page 1]. NPO-20696



Materials

Hardware, Techniques, and Processes

- 27 Antioxidant Fiber Finishes for Polyimide-Matrix Composites
- 27 High-Performance Zn Anodes for Ag/Zn and Ni/Zn Cells
- 28 Enhanced Shield Against Meteoroids and Orbital Debris

Books and Reports

- 29 Update on a Progressive-Failure-Analysis Software System

26

BLANK PAGE

Antioxidant Fiber Finishes for Polyimide-Matrix Composites

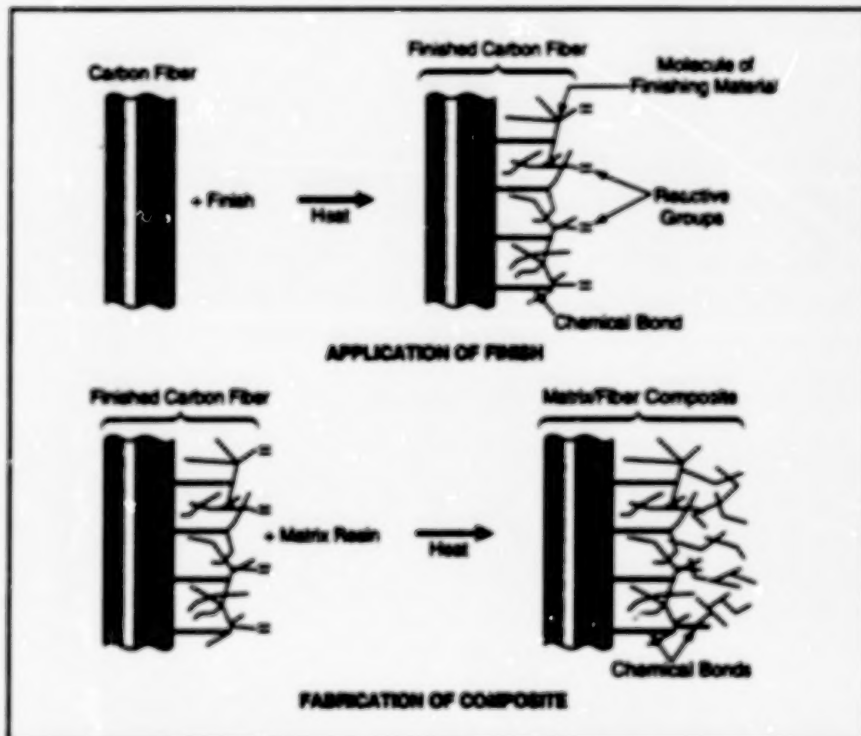
These are reactive finishes that increase thermo-oxidative stability.

John H. Glenn Research Center,
Cleveland, Ohio

Polyimide-matrix/carbon-fiber composite materials with enhanced thermo-oxidative stability can be made from carbon fibers that have been coated with suitably formulated reactive finishing materials. These finishing materials were developed out of a need to increase thermo-oxidative stability of composite materials for high-temperature applications, and in response to the observation that thermo-oxidative degradation of polyimide-matrix/carbon-fiber composites is dominated by phenomena that occur at matrix/fiber interfaces.

The figure schematically depicts the coating of a carbon fiber with a reactive finish and the subsequent incorporation of the fiber into a polyimide-matrix/carbon-fiber composite. Reactive coupling agents in the finishing material chemically bond to both the carbon fibers and the polyimide resin. The fiber/finish and finish/matrix chemical bonds increase the durability of the composite material by strongly resisting attack by oxygen, moisture, and solvents. The chemical bonds also increase interfacial strength and resistance to fatigue.

The finishing material includes a resin carrier compatible with the matrix resin. By selection of different carrier resins, it should be possible to formulate other reactive finishes and tailor interfacial properties, not only for polyimides, but also for a variety of other matrix materials, including epoxies, bismaleimides, phenolics, vinyl esters, and polyesters.



A Reactive Finish is applied to a carbon fiber, with which it forms a chemical bond. During the subsequent incorporation of the fiber into a composite material, the finish forms a chemical bond with the matrix.

This work was done by James K. Sutter of Glenn Research Center and Ronald E. Alfred and Larry A. Harrah of Adherent Technologies, Inc. Further information is contained in a TSP [see page 1].

Inquiries concerning rights for the com-

mmercial use of this invention should be addressed to NASA, Glenn Research Center, Commercial Technology Office, Attn: Steve Fedor, Mail Stop 4-8, 21000 Brookpark Road, Cleveland, Ohio 44135. Refer to LEW-16729.

High-Performance Zn Anodes for Ag/Zn and Ni/Zn Cells

Cycle lives are increased and costs are reduced.

Lyndon B. Johnson Space Center,
Houston, Texas

Improved zinc anodes for silver/zinc and nickel/zinc rechargeable electrochemical cells have been invented. This invention will increase the usefulness and decrease cycle-life costs of Ag/Zn and Ni/Zn cells in NASA Space-Station-support applications, for which batteries with high energy densities and long cycle lives are needed; examples of these applications include extravehicular mobility unit (EMU) batteries, the EMU portable life-support subsystem (PLSS) backpack batteries, and batteries in portable tools and equipment for extravehicular activities (EVAs). Inasmuch as many of these

portable tools and other items of equipment are modified versions of commercial items (portable tools, lights, cameras, recorders, camcorders, radios, communications equipment, cellular telephones, and medical equipment), this invention might also prove beneficial in numerous commercial applications. Similarly, it could offer benefits in military applications, other government applications, and other applications that involve batteries.

Two phenomena that limit the cycle lives of Ag/Zn and Ni/Zn secondary cells were unaddressed prior to this invention. These phenomena are (1) gradual changes in the

shapes of zinc electrodes and (2) the deposition of zinc as dendrites during recharge.

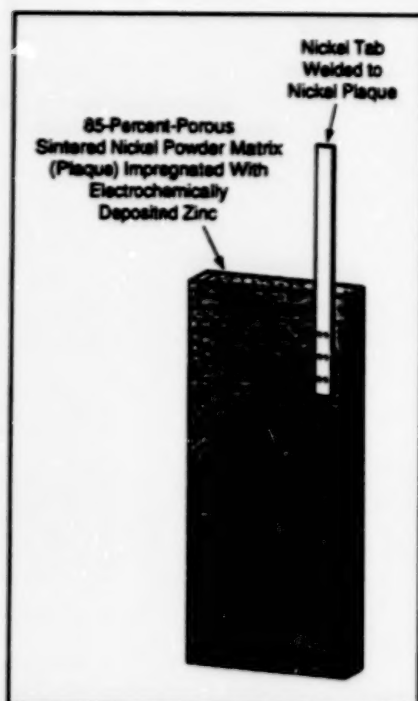
- Regarding the shape changes: During charge/discharge cycling, the anodes become denser and lose active surface area. These changes cause progressive losses of capacity and thus of cycle life.
- Regarding the dendrites: These are sharp, needlelike crystals, which can penetrate cell separators and thereby cause internal short circuits.

Either phenomenon can lead to an uncomfortable, even a hazardous situation during a space flight. The invention maintains the integrity of a nickel anode,

helping to prevent both of these phenomena. In so doing, it increases cycle life and thereby reduces the cost per cycle.

A typical conventional commercial zinc electrode contains a conductive grid made of perforated or expanded metal (typically copper) sheet. The invention involves a different approach: a zinc electrode according to the invention can be manufactured in a manner similar to that of making cadmium electrodes for aerospace cells. A porous sintered nickel powder matrix (plaque) is loaded with zinc by immersing the sinter in a zinc nitrate solution and electrochemically reducing the zinc. When the resulting anode is assembled into a battery, the form of the anode (see figure) is maintained by the nickel matrix. Even though nickel can give rise to excessive gassing by electrocatalyzing the decomposition of water, the use of nickel nevertheless confers an advantage by reducing the incidence of dendritic shorting and thereby extending cycle life.

Calculations have shown that the energy density of a cell is not impaired by substituting the zinc-loaded nickel-plaque anode for a conventional copper-grid-supported anode. Calculations have also shown that



A High-Performance Zinc Anode includes a porous nickel plaque that maintains its size and shape. The active anode material (zinc) is loaded into the pores.

the plaque, when loaded with the same weight of zinc that would be included in a conventional anode, accommodates the increased volume of zinc oxide that is generated during discharge.

It has been suggested in some quarters that high-performance zinc anodes might be improved through use of a copper plaques of the proper porosity. However, there is no substantive evidence that this option would yield a greatly enhanced cycle life or address the shape-change and dendrite issues. Therefore, despite lower porosity (85 percent) of the nickel plaque relative to the 90-percent porosity of copper plaque, nickel plaque was chosen over copper plaque.

This work was done by John E. Casey of Lockheed Engineering & Sciences Co. for Johnson Space Center. Further information is contained in a TSP [see page 1].

This invention has been patented by NASA (U.S. Patent No. 5,780,186). Inquiries concerning nonexclusive or exclusive license for its commercial development should be addressed to the Patent Counsel, Johnson Space Center, (281) 483-0837. Refer to MSC-22540.

Enhanced Shield Against Meteoroids and Orbital Debris

This shield significantly decreases the likelihood of loss of a crew and/or spacecraft.

Lyndon B. Johnson Space Center,
Houston, Texas

NASA scientists, who are very concerned with the increasing hazard of impacts of orbital debris impact on spacecraft, have designed the "stuffed Whipple" shield — a lightweight, relatively inexpensive alternative to simple aluminum meteoroid/orbital-debris (M/OD) shield. The stuffed Whipple shield features an easily adaptable design that increases protection against hypervelocity impacts (HVIs), without significantly affecting previously formulated designs of spacecraft. The stuffed Whipple shield is critical to the continued human exploration of space, especially to the Space Station, inasmuch as the Station will be operating in low orbit around the Earth and will need shielding against HVIs in order to survive intact and for an appreciable amount of time and continue to safely support human habitation. Scientists project that the number of HVIs from detritus of artificial objects will increase from 2 to 5 percent per year — an increase that could produce devastating results.

The design of the stuffed Whipple shield greatly reduces the risk of loss of a spacecraft crew and/or damage to the spacecraft. It also increases crew efficiency, in

that by providing more efficient shielding, it reduces the frequency of both extravehicular and intravehicular activities EVAs and NAs to effect repairs of HVI penetrations of the outer skin of the spacecraft. It is particularly amenable to introduction in the final or nearly-completed phase of the spacecraft-design effort. The stuffed Whipple shield can be retrofitted to any extant military or commercial spacecraft.

Many previously designed space vehicles are equipped with all-aluminum shields, of a form of Whipple shield, for protection against HVIs. All-aluminum shields offer an improvement over shields of the earliest designs; however, all-aluminum shields were designed for a situation in which an HVI, while always a possibility, seemed a remote likelihood. Indeed, even the earlier Space Station designs were completed before emergence of the awareness of the artificial-debris environment and of the consequent need for greater protection, and at greater cost savings.

As the orbital-debris environment affects more commercial satellites, there will be a need to add lightweight anti-HVI

shielding for protection. By virtue of its incorporation of lightweight materials and its easily adaptable design, the stuffed Whipple shield can be used on Space Station pressurized modules and on any spacecraft that typically carries a simple aluminum M/OD shield.

Better yet, the reduction in launch weight afforded by replacing the all-aluminum shield with the stuffed Whipple shield results in an estimated reduction of \$345 M in the cost of launch. It is not surprising, therefore, that increased safety and decreased cost equally drive the stuffed-Whipple-shield design for the Space Station.

A stuffed Whipple shield includes front and back sheets and contains lightweight materials (the "stuffing"). The stuffing materials are selected and placed so as to break up large impinging particles, stop small impinging particles, and decelerate debris clouds before they can reach the back sheet. (In the case of the habitable Space Station modules, the back sheets are the pressure shells of the modules.)

A stuffed Whipple shield also offers a secondary support structure, which

reduces system costs. This secondary structure is a mesh/Nextel (or equivalent ceramic)/Kevlar (or equivalent aromatic polyamide) blanket that can be supported in a number of ways. For example, it can be held by brackets, frames, or other supports that are modified versions of supports used in the current Space Station design to attach multilayer thermal insulation blankets. Another method of support involves mounting

the blanket on a rigid graphite/epoxy or aromatic-polyamide/epoxy panel; the panel is then attached to the previously installed bumper-support structure, where its rigidity can potentially be offset by reductions in the blanket (i.e., the aromatic polyamide portion).

This work was done by Jeanne L. Crews and Eric L. Christiansen of Johnson Space Center and Joel E. Williamsen, Jennifer H. Robinson, and

Angela M. Nolen of Marshall Space Flight Center. Further information is contained in a TSP [see page 1].

This invention has been patented by NASA (U.S. Patent No. 5,610,363). Inquiries concerning nonexclusive or exclusive license for its commercial development should be addressed to the Patent Counsel, Johnson Space Center, (281) 483-0837. Refer to MSC-22584.

Books and Reports

Update on a Progressive-Failure-Analysis Software System

A report presents additional information on the GENOA-PFA computer program, which was described in "Software for Simulating Progressive Fracture in Braided PMCs" (LEW-16845), *NASA Tech Briefs*, Vol. 24, No. 3 (March 2000), page 52. On the basis of material-property data, finite-element mathematical models, and service conditions, GENOA-PFA simulates the initiation and progression of damage ultimately leading to global structural failures in composite-material structures. The composite materials include complex architec-

tures in which fibers are placed in two- or three-dimensional weaves or braids. Whereas the cited prior article characterized GENOA-PFA as applicable to only polymer-matrix composites, the report characterizes it as applicable to other composite structures also, including ones that contain ceramic or metal matrices. The report expands on the capabilities of GENOA-PFA and its applicability to various problems; in this regard, the report emphasizes the utility of GENOA-PFA as means of "virtual testing" — that is, as a time- and cost-reducing computational substitute for preliminary experimental testing of material specimens to accelerate and facilitate the evaluation of numerous iterations of the

design of a composite-material structure.

This work was done by Pappu L. N. Murthy and Christos C. Chamis of Glenn Research Center, Frank Abdi of Alpha Star Corp., and Levon Minnetyan of Clarkson University. To obtain a copy of the report, "GENOA a Progressive Failure Analysis Software System," see TSP's [page 1].

Inquiries concerning rights for the commercial use of this invention should be addressed to NASA Glenn Research Center, Commercial Technology Office, Attn: Steve Fedor, Mail Stop 4-8, 21000 Brookpark Road, Cleveland, Ohio 44135. Refer to LEW-16858.



Mechanics

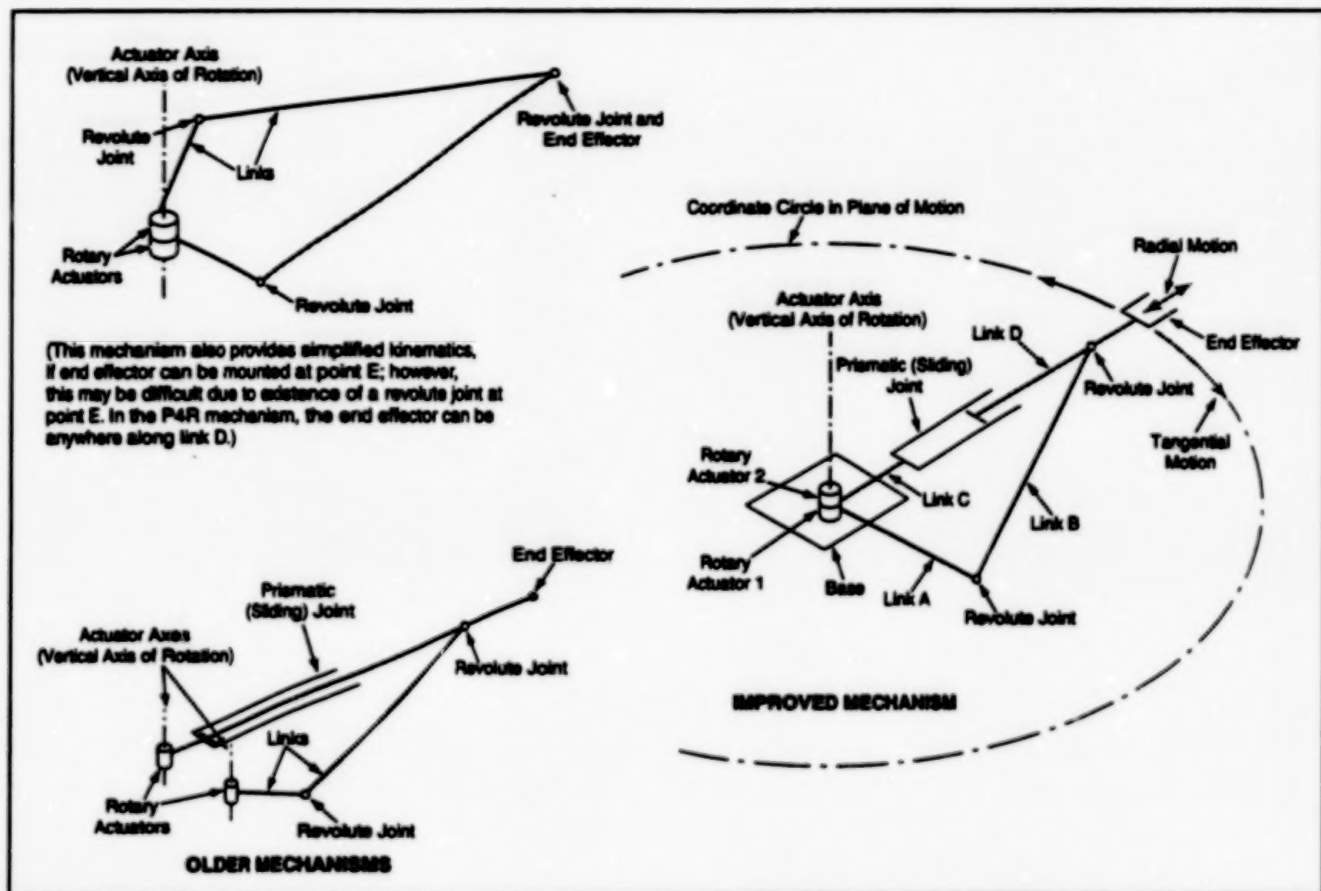
Hardware, Techniques, and Processes

- 33 Mechanism for Planar Manipulation With Simplified Kinematics
- 34 Improved Cable-Drive Pretensioner
- 34 Tape-Spring Reinforcements for Inflatable Structural Tubes
- 35 Mechanism for Adjusting and Measuring Tension in a Cable
- 35 Electromechanical Testing of Microelectromechanical Devices

Mechanism for Planar Manipulation With Simplified Kinematics

Simple combinations of actuator motions yield purely radial or purely tangential end-effector motions.

Goddard Space Flight Center,
Greenbelt, Maryland



The improved mechanism affords a simplification of kinematics: Whereas the coordination of actuator motions necessary to obtain specified end-effector motions in the older mechanisms is a complex task, it is a relatively simple task in the improved mechanism.

The figure schematically illustrates three manipulator mechanisms for positioning an end effector (a robot hand or other object) in a plane (which would ordinarily be horizontal). One of these is a newer, improved mechanism that includes two coaxial, base-mounted rotary actuators incorporated into a linkage that is classified as "P4R" in the discipline of kinematics of mechanisms because it includes one prismatic (P) joint and four revolute (R) joints. The improved mechanism combines the advantages of coaxial base mounting (as opposed to noncoaxial and/or nonbase mounting) of actuators, plus the advantages of closed-loop (as opposed to open-loop) linkages in such a way as to afford a simplification (in comparison with other linkages) of inverse kinematics. Simplification of the kinematics reduces the computational burden incurred in controlling the manipulator.

In the general case of a two-degree-of-freedom manipulator with two rotary actuators, the inverse kinematic problem is to

find the rotary-actuator angles needed to place the end effector at a specified location, velocity, and acceleration in the plane of motion. In the case of a typical older manipulator mechanism of this type, the solution of the inverse kinematic problem involves much computation because what one seeks is the coordinated positions, velocities, and accelerations of the two manipulators, and these coordinates are kinematically related to each other and to the required motion in a complex way.

In the improved mechanism, the task of coordination is greatly simplified by simplification of the inverse kinematics; the motion of the end effector is easily resolved into a component that is radial and a component that is tangential to a circle that runs through the end effector and is concentric with the rotary actuators.

If rotary actuator 2 is held stationary, while rotary actuator 1 is turned, then link D slides radially in the prismatic joint, causing the end effector to move radially. If both rotary actuators are turned togeth-

er, then there is no radial motion; instead, the entire linkage simply rotates as a rigid body about the actuator axis, so that the end effector moves tangentially. Thus, the task of coordination is reduced to a simple decision to (a) rotate actuator 1 only to obtain radial motion, (b) rotate both actuators together to obtain tangential motion, or (c) rotate the actuators differentially according to a straightforward kinematic relationship to obtain a combination of radial and axial motion.

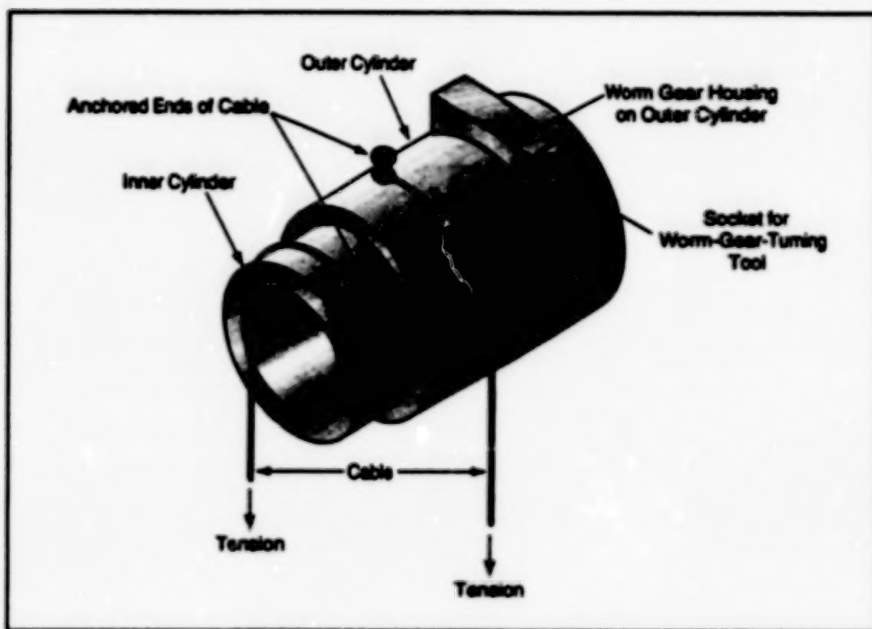
This work was done by Farhad Tahmasebi of Goddard Space Flight Center. Further information is contained in a TSP [see page 1].

This invention is owned by NASA, and a patent application has been filed. Inquiries concerning nonexclusive or exclusive license for its commercial development should be addressed to the Patent Counsel, Goddard Space Flight Center [see page 1]. Refer to GSC-13655.

Improved Cable-Drive Pretensioner

Tension is adjusted easily by use of a worm gear.

Lyndon B. Johnson Space Center,
Houston, Texas



Tension in the Cable is Adjusted by turning one cylinder relative to the other. In the improved mechanism, this is done by use of a worm-gear drive.

An improved mechanism has been devised to facilitate the adjustment of tension in a cable in a cable-and-pulley drive. Cable-and-pulley drives are being used increasingly in robots and other high-performance, computer-controlled machines. Typically, a cable is looped around various drive pulleys with its ends anchored in proximity to each other on two coaxial cylinders (see figure). During operation of the cable drive, the cylinders are locked

against rotation relative to each other to maintain a preset tension. To adjust the tension, it is necessary to unlock the cylinders and rotate them relative to each other.

In a typical older cable-tensioning mechanism, lock between cylinders is maintained by set screws. To adjust tension, it is necessary to loosen the set screws, turn the cylinders slightly to obtain the desired tension, then tighten the set screws. This procedure is tedious and labor-intensive;

sometimes it requires as many as three technicians working simultaneously with three wrenches and a screwdriver. If one of the technicians slips, it is necessary to repeat the procedure and, depending on the design of the particular cable drive, it could be necessary to dismount and remount the cables.

The improved mechanism is both a locking and an adjustment mechanism that can be adjusted easily by one technician. In this mechanism, the cylinders are turned relative to each other by use of a worm-gear drive. The outer cylinder houses the worm, while the mating worm gear is attached to the inner cylinder. A technician turns the worm by use of a hand tool. There is no need to provide explicitly for locking against inadvertent or undesired relative rotation: the friction inherent in the worm-gear drive prevents backdriving under cable tension.

This work was done by William Townsend of Barrett Technology, Inc., for Johnson Space Center. Further information is contained in a TSP [see page 1].

In accordance with Public Law 96-517, the contractor has elected to retain title to this invention. Inquiries concerning rights for its commercial use should be addressed to

Barrett Technology, Inc.
545 Concord Avenue
Cambridge, MA 02138

Refer to MSC-22405, volume and number of this NASA Tech Briefs issue, and the page number.

Tape-Spring Reinforcements for Inflatable Structural Tubes

Tape-springs and tubes help each other resist buckling.

NASA's Jet Propulsion Laboratory,
Pasadena, California

Lightweight, inflatable tubular structural components containing tape-spring reinforcements are undergoing development. The basic (without tape-spring reinforcement) tubular components are made, variously, of aluminum laminates or composite materials and are under consideration for use in erecting structures in outer space. They could also be used to erect structures for terrestrial applications in situations in which a greater value is placed in light weight than on strength.

Two types of tape-spring reinforcements have been conceived for this purpose: longitudinal and circumferential.

Longitudinal tape-spring reinforcements are made from strips of spring steel or other high-modulus materials with curved cross sections, such as the type of spring strips used commonly in compactly stowable carpenters' measuring tapes. The reinforcements would exploit the well known nonlinear mechanical responses of such tapes, namely: (1) high resistance to buckling while they are straight, (2) the ease with which they can be rolled up once they have been initially flattened, and (3) much stronger resistance to bending or buckling toward the concave-side-out configuration than toward the

concave-side-in configuration.

Usually, a thin-wall tube buckles inward first. If one attaches longitudinal curved-cross-section tape springs to the inside of a thin-wall tube at several circumferential positions and orients them with their concave sides facing toward the interior, then the tape-springs help to restrain the tube against inward buckling while the tube helps to restrain the tapes against outward buckling. The net effect is a large increase in the load-bearing capacity of the reinforced tube.

Because the stiffness of a tape-spring decreases as its length increases, it has

been proposed to add circumferential reinforcing tape-springs, or other forms of circumferential reinforcement, to long tubes for certain applications. Circumferential reinforcing tape-springs would be fabricat-

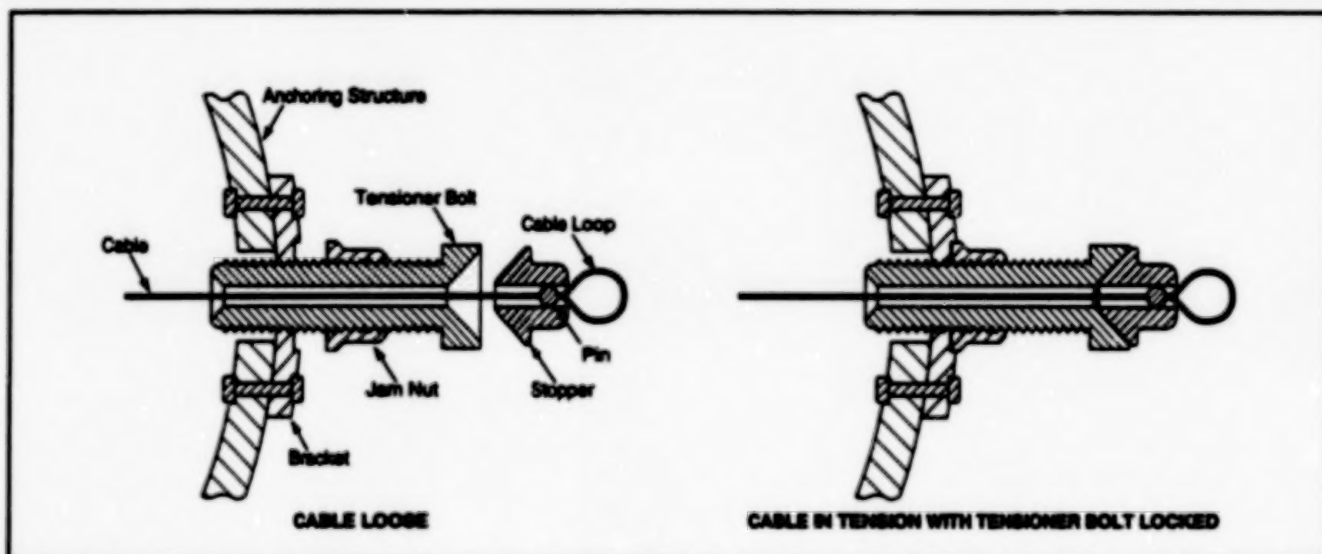
ed as straight, thin, flat strips. They would be attached to the insides of the tubes. The circumferential reinforcements would also serve as hard attachment points for tubes subjected to lateral loading.

This work was done by Houlei Fang and Michael Lou of Caltech for NASA's Jet Propulsion Laboratory. Further information is contained in a TSP [see page 1].
NPO-20615

Mechanism for Adjusting and Measuring Tension in a Cable

Where measurement is necessary, this mechanism could be preferable to a turnbuckle.

Lyndon B. Johnson Space Center,
Houston, Texas



The Tension in the Cable is Adjusted by turning the tensioner bolt. The tensioner bolt can be locked by use of the jam nut. The tension can be measured by pulling on the cable loop.

The figure illustrates a simple mechanism designed for anchoring one end of a cable on a structure and for adjusting the tension in the cable. Unlike turnbuckles and other conventional cable-tensioning mechanisms, this mechanism also facilitates direct measurement of the tension in the cable. Several of these mechanisms are used in concert in order to suspend a structure for thermal isolation.

The bracket is used to secure the mechanism to the anchoring structure.

The near end of the cable is threaded through the mechanism and tied off in a loop at the pin in the stopper. The tensioner bolt is turned counter-clockwise in the bracket until the bored conical hole at its outer end mates with the conical surface of the stopper, placing the cable in tension.

Further counter-clockwise rotation of the tensioner bolt increases the tension. The tension can be measured directly by simply pulling on the cable with a force

gauge; the tension equals the measured force that is just sufficient to unseat the stopper. Once the specified tension has been achieved, the tensioner bolt is locked in place by tightening the jam nut against the bracket.

This work was done by Ross G. Iacomini of Johnson Space Center. Further information is contained in a TSP [see page 1].
MSC-22704

Electromechanical Testing of Microelectromechanical Devices

Devices would be probed at the wafer level before dicing and packaging.

NASA's Jet Propulsion Laboratory,
Pasadena, California

A method of electromechanical testing has been proposed for general diagnosis, evaluation of performance, and burn-in (accelerated life testing) of microelectromechanical devices. The tests would ordinarily be performed at the wafer level; that is, after the devices have been fabricated on wafers but before the wafers have been diced and the dies packaged. Alternatively or in addition, the tests could be performed at other stages of the fabri-

cation process.

According to this method, a probe would apply a specified mechanical and/or electrical stimulus to each device (sensor or actuator) on a wafer, and the response of the device to the stimulus would be measured. The things most likely to be useful as probes are piezoelectric transducers because they are easy to use, rugged, and compact and they have wide dynamic ranges.

A piezoelectric transducer can function as a driver, a force-measuring sensor, or both simultaneously. The displacement or change of thickness of a piezoelectric crystal is proportional to the voltage applied across it. If the voltage applied to a piezoelectric crystal oscillates sinusoidally with time, then the amplitude of the acceleration is proportional to the applied voltage and to the square of the oscillation frequency. In that case, the force exerted by the crystal on a tested

device is related to the amplitude and phase of the electrical impedance of the crystal.

If sinusoidal excitation were used, the ratio between the force applied to, and the resultant acceleration of, a tested device would be a complex impedance quantity that could be characterized as the effective mass of the device; the effective mass would reflect the mass, stiffness, and damping characteristics of the device. If the device were an accelerometer or pressure transducer, then the effective mass would include the proof mass (in the case of the accelerometer) or the mass of the diaphragm (in the case of the pressure transducer); the effective mass could also include part of the mass of a

housing and/or the masses of other structures that participate in motion.

Piezoelectric transducers for testing the devices on a wafer could be assembled into a probe station. Typically, each probe would contain a piezoelectric crystal that had a specified thickness and a flat and smooth contact surface that would match the portion of the wafer area occupied by a die containing a device to be tested. The probe would be fixed to a probe platform with an elastomeric material. Electrical connection buttons would also be suspended in the elastomeric material. The piezoelectric crystal and connection buttons would be aligned with the die before lowering the probe platform and thereby

compressing elastomer and preloading the crystal. The compressive preload would be made large enough to prevent the loss of compressive load on the crystal at any stage of the test process.

Once the preload was applied, testing could begin. The resonance frequencies, damping rates, and performance parameters of the devices on the wafers could be measured. Accelerated life testing could be performed by stimulating the devices at their resonances for extended times.

This work was done by Frank Hartley of Caltech for NASA's Jet Propulsion Laboratory. Further information is contained in a TSP [see page 1].
NPO-20563



Machinery

Hardware, Techniques, and Processes

39 Path-Planning Program for a Redundant Robotic Manipulator

Path-Planning Program for a Redundant Robotic Manipulator

This program utilizes kinematic redundancy to find singularity-free, obstacle-avoiding paths.

Lyndon B. Johnson Space Center,
Houston, Texas

The Space Station Robot Manipulator System (SSRMS) Path Planning Program is a computer program that, in comparison with software developed previously for the same purpose, supports operations of faster and more complex robots. Two especially notable features of the program are that (1) it makes for ease of description of the work space of a remote manipulator or other robot and (2) it takes advantage of redundant degrees of freedom of the manipulator by finding manipulator-link paths that avoid both mathematical singularities and physical obstacles. The program can be applied not only to space-station manipulators and other robots but also to manipulators and other robots used in remediation of waste sites and demanding nuclear facilities. With moderate modifications, the program could even be used in reconfigurable manufacturing operations.

In the original International Space Station application, there is a need to assure the safety of the crew and equipment by calculating a safe path and an optimal trajectory for the SSRMS, which has seven degrees of freedom (DOFs). In the absence of the present or a similar program, determining a safe path through a field of obstacles is difficult because the end-effector trajectory and the necessary manipulator-joint-angle trajectories must be taken into account manually; as a consequence, the chosen path may not be the optimal path. The SSRMS Path Planning Program automates the path-planning process. It searches for, and finds, the optimal trajectory in a matter of seconds.

The idea for the program came from R. V. Mayorga, who proposed a path-planning method for a manipulator that is redundant in the sense that the number of its DOFs exceeds the number of task elements. An analysis of the method was performed for a 3-DOF manipulator oper-

ating in a plane; then the analysis was extended to a 7-DOF manipulator operating in three-dimensional space. Finally, all the equations of the method specific to the SSRMS were formulated, together with some clever ways of incorporating them into a computer code. The SSRMS Path Planning program, written in ANSI-C, evolved from this final analysis.

The SSRMS Path Planning Program follows the artificial-potential-field approach to planning the path of the end effector of the remote manipulator. Real-time joint-angle trajectory planning for enabling manipulator links to avoid obstacles, involving the use of a null-space vector, is implemented in this program. All of the equations of kinematics and inverse kinematics specific to the SSRMS are also included.

In Mayorga's method, the goal configuration is represented by an attractive potential and obstacles by repulsive potentials. The determination of the manipulator joint-angle trajectory involves the inversion of a potential-field matrix, but this is subject to difficulties when the manipulator approaches singular configurations. With respect to singular configurations, the SSRMS Path Planning Program incorporates two improvements: (1) the manipulator trajectory is determined directly from the gradient of the potential field, so that there is no need to invert nearly singular matrices; (2) a global perspective is added by providing for the predetermination of optimal (shortest-path) goal trajectory for the end-effector position. The attractive potential is then based on an optimal trajectory that guides the end effector around obstacles in the shortest possible distance.

The program reads two input files. The first file describes the work space; the second file contains constants, integration parameters, the initial configuration, and the goal configuration. From these inputs, the

program calculates a path through the work space, going from the initial configuration to the goal configuration along a path that avoids obstacles for the end effector and the manipulator links. By varying the values of some or all of the constants, one can change a path to incorporate a wider or narrower clearance of obstacles, change the time to complete the task, and/or otherwise alter the nature of the task. The joint-angle trajectories are computed by another program, "PLUMECHCK," on a Silicon Graphics workstation. PLUMECHCK can display animation of the manipulator arm.

The SSRMS Path Planning Program is an improvement over programs developed previously for the same purpose in the following respects:

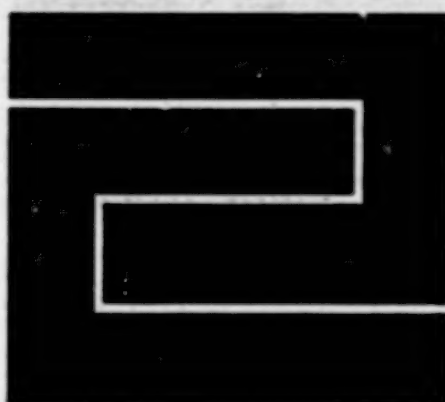
- Path planning has been automated. The joint-angle trajectories for any path can be found in seconds. Therefore, many different scenarios can be tried to find an optimal path.
- It is easy to describe the work space, including obstacles, forbidden regions, and other important features of the work space.
- The redundancy of the SSRMS is not a disadvantage for this program; on the contrary, it is an advantage when there is a need to find singularity-free paths and avoid obstacles.

The SSRMS Path Planning Program has much to recommend it. Its potential field-based approach to avoidance of collisions by kinematically redundant manipulators has already been demonstrated in research laboratories. This program is being evaluated with respect to commercial applicability.

This work was done by Glenn V. Webb of Rockwell Space Operations for Johnson Space Center.
MSC 22751

4

BLANK PAGE



Fabrication Technology

Hardware, Techniques, and Processes

43 Maskless Gray-Scale X-Ray Lithography

42

BLANK PAGE

Maskless Gray-Scale X-Ray Lithography

Spatial variations in exposure of photoresist would be effected through variations in scan rates.

In a proposed technique of maskless gray-scale x-ray lithography, a photoresist to be patterned would be exposed to a parallel beam of hard x rays. As explained below, the photoresist would be translated across the beam at a varying rate to effect one-dimensional spatial variations in the radiation dose received by the photoresist. The technique would be particularly suitable for making diffraction gratings and similar items.

In gray-scale lithography in general, the radiation dose to a photoresist on a substrate is made to vary spatially, within a range in which the solubility of the exposed photoresist in a developer liquid varies with the dose. In customary gray-scale x-ray lithography, the required spatial variation in the dose is achieved by use of a mask. The mask and the photoresist-covered substrate are translated as a unit across an x-ray beam at a constant rate to obtain

the required integrated dose to the mask.

The lithographically desirable characteristics of a parallel beam of hard x rays include a large depth of field (typically characterized by image dispersion less than 1 μm over a depth of 15 mm) and negligible reflections from photoresist defects and surfaces. A parallel beam of hard x rays (wavelengths $< 10 \text{ \AA}$) for use in the proposed technique could be generated by a synchrotron source in conjunction with a slit filter (typically 50 nm wide).

In the proposed technique, the photoresist would not be masked. The gradients in the radiation dose needed to obtain gradients in the density of the developed photoresist would be generated by controlled variations in the rate of translation of the x-ray beam across the photoresist. These controlled variations would suffice to define the desired features (variations of the height of the subsequently developed photoresist)

NASA's Jet Propulsion Laboratory,
Pasadena, California

to within submicron dimensions, within the 15-mm depth of field.

After exposure to x-rays, the photoresist would be developed in the customary manner. After development, the photoresist would be dried, giving rise to spatial consolidation of the photoresist into thickness gradients corresponding to the density gradients. The dosage gradients could be chosen to achieve desired final thickness gradients; for example, to produce triangular- or sawtooth-cross-section blazes for diffraction gratings. The large depth of field could be exploited to form such blazes on curved surfaces.

This work was done by Frank Hartley of Caltech for NASA's Jet Propulsion Laboratory. Further information is contained in a TSP [see page 1].
NPO-20445

44

BLANK PAGE



Mathematics and Information Sciences

Hardware, Techniques, and Processes

- 47 Software Facilitates Access to a Scientific Data Base
- 47 Software Improves Management of Dynamic Memory
- 48 A Standard for Scientific Data Files
- 48 Software for Display and Analysis of Scientific Data

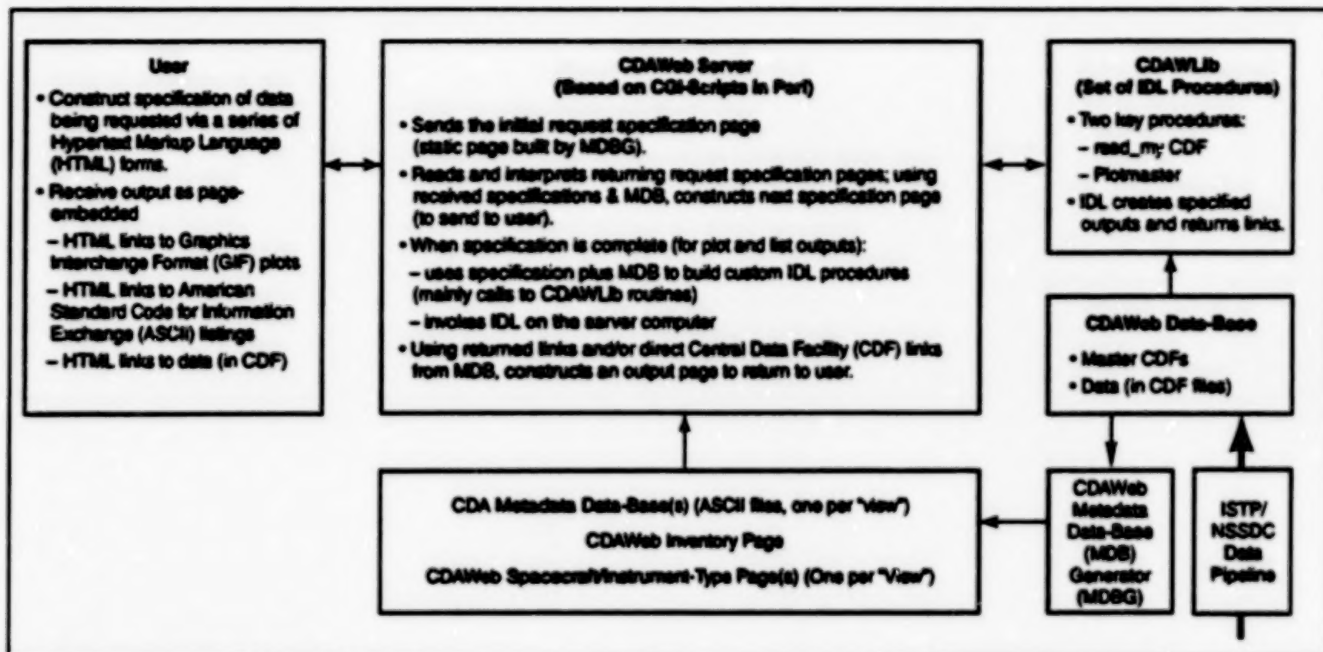
46

פסוקי דשמוע

Software Facilitates Access to a Scientific Data Base

This program supports cooperative international scientific efforts.

Goddard Space Flight Center,
Greenbelt, Maryland



CDAWeb Assists the User in obtaining scientific data that have been stored in a prescribed format.

The Coordinated Data Analysis Workshop Web (CDAWeb) is a web-based service that facilitates access to a scientific data base of the International Solar-Terrestrial Physics (ISTP) program and other programs that generate public scientific information. In this data base, physical-science parameters from diverse international sources are stored in the Common Data Format (CDF) standard developed by the National Space Science Data Center (NSSDC).

The data of the ISTP program and the CDAWeb service are parts of NASA's contribution to the Solar-Terrestrial Science

Initiative of the Inter-Agency Consultative Group (IACG), a multinational space-science coordinating group. Under the auspices of IACG, CDAWeb mirror sites have been established at the Equator-S science center at the Max-Planck Institute in Garching, Germany, and at the Rutherford Appleton Laboratory in the United Kingdom.

CDAWeb is built using standard software packages. The "engine" of CDAWeb is a set of scripts in the Interactive Data Language (IDL) of Research Systems Inc. (RSI). CDAWeb also includes web-page software components and common gate-

way interface (CGI) scripts that act as interfaces between the IDL scripts and the user, plus supporting software utilities to create the metadata data-base files used by the interface scripts. The CDAWeb software package for mirror sites does not include IDL, which is a commercial product that must be obtained separately.

This work was done under the direction of Robert E. McGuire of Goddard Space Flight Center. For further information, access the CDAWeb service at <http://cdaweb.gsfc.nasa.gov> or see TSP's [page 1].
GSC-14292

Software Improves Management of Dynamic Memory

This software increases efficiency in the allocation and use of storage space.

Marshall Space Flight Center,
Alabama

The Dynamic Memory Management System (DMMS) is a computer program that was developed in response to some major shortcomings of dynamic-memory-management subsystems of typical operating systems. It is designed for use with the VxWorks operating system, but is easily ported to other operating systems.

The shortcomings in question are the following:

- Memory fragmentation — the waste of storage space that occurs when many small blocks of storage space (buffers)

are scattered randomly throughout a memory pool and the memory-management component of software is unable to coalesce these small buffers into a larger buffer;

- Memory leak — progressive loss of storage space that occurs because an error in the storage-allocation component of software causes a failure to deallocate memory space that is no longer needed for the task at hand;
- Limited or no visibility into usage of dynamic memory; and

- Unreported overwriting of allocated memory buffers.

DMMS is designed to overcome these shortcomings while maintaining a simplistic interface and providing rapid execution. DMMS offers the advantages of the core memory-partition-manager component of VxWorks; namely, ease of implementation and rapid (taking tens of microseconds or less in typical cases) allocation and deallocation of buffers. DMMS enables monitoring of usage of dynamic memory and integrity of dynamic memory at buffer-release time;

these features enable the user to fine-tune DMMS to obtain the highest possible performance and to become aware of gaps in the integrity of dynamic data buffers.

Going beyond what is offered by VxWorks, DMMS offers the following additional features:

- Memory is allocated according to the buddy system instead of a first-fit algorithm. In the buddy system, buffers are allocated in sizes that are always powers of two, so that they can readily be joined and/or split. Unused smaller buffers that have been made by splitting larger ones are made available for allocation. The net effects of the buddy system are to pre-

vent fragmentation of the memory pool and to contribute to rapidity of allocation and deallocation.

- Freed blocks are coalesced only when necessary and only to the extent necessary. This practice offers a timing advantage over the older practice of coalescing buffers as much as possible whenever a buffer is freed.
- The user is notified of writing data past the end of a buffer when deallocation of the buffer is requested. During development, such overwriting is a frequent error that is sometimes difficult to identify without the help of this feature of DMMS.
- The identity of the task that requested a

dynamic buffer is made known. This information can be helpful in finding and correcting a software component that causes memory leak.

- Information on the "high-water usage" (maximum number used) of buffers of each size is made available. This information can be used in fine tuning to reduce the size of the overall dynamic buffer pool.

This work was done by Ron Phillips of Sverdrup Technology, Inc., for Marshall Space Flight Center. For further information, please contact Sverdrup Technologies, Inc., 620 Discovery Drive, Huntsville, AL 35806, Telephone No. (256) 971-9425. MFS-31287

A Standard for Scientific Data Files

This standard and the software that implements it facilitate collaboration among scientists.

The term "Instrument Data File Set" (IDFS) denotes both software and an underlying concept of a prescribed format for files of scientific data and metadata. The IDFS was developed to satisfy a need, in the space science community, to maintain data and metadata in a format that promotes efficient use of the information and that facilitates access to the information, thereby enhancing the ability of scientists to engage in collaborative research. Within the space science community, the IDFS has become a standard by default.

Metadata, which accompany scientific measurement data, can include information about formats of measurement data,

parameters of scientific instruments, calibration tables, tables for conversion of measurement data to scientific units of measurement, timing factors, and other information that does not necessarily originate from scientific instruments but is necessary for research. The IDFS software provides easy access to IDFS-formatted data via a catalog subsystem and data access routines. The catalog subsystem contains information about which IDFS-formatted data are available for use. The data access routines extract IDFS-formatted data in a variety of ways for meaningful presentation.

The IDFS concept and software addresses the deficiencies of other meth-

ods for the storage and representation of space science data. Two key tasks that can be performed with the help of the IDFS software are the conversion of telemetry values to engineering and scientific units and the registration of each datum with a given point in time; in this respect, the IDFS enables efficient presentation of the data from simultaneous measurements made on different instruments.

This work was done by Carrie Gonzalez, Joey Mukherjee, and Sandee Jeffers of Southwest Research Institute for Marshall Space Flight Center. For more information, contact the Southwest Research Institute at (210) 522-2010. MFS-31325

Marshall Space Flight Center,
Alabama

Software for Display and Analysis of Scientific Data

Data can be obtained from globally distributed archives, then displayed and analyzed quickly.

The Southwest Data Display and Analysis System (SDDAS) is a flexible, extensible software system intended to support analysis of space physics data from multiple instruments and multiple spacecraft missions. SDDAS was developed in response to the need of space scientists to be able to gain access to data and to display data, without concern about data management details, so that they can focus their efforts on scientific research.

SDDAS gives the scientists a software "toolbox" that can bridge the gap between data and scientific insight. SDDAS makes it possible to quickly display and analyze data in distributed archives from many different satellites and other sources by use of a diverse set of graphical application

programs. Data can be ordered and delivered over the Internet, independently of the locations of archives and of the nature of the archival storage.

The graphical software tools are the heart of SDDAS and are oriented toward the examination of data in the Instrument Data File Set (IDFS) format, which is the subject of the preceding article. The development of SDDAS has been "bottom-up" rather than "top-down" and user-driven rather than organization-driven. SDDAS is adaptable to advances in computer technology; that is, it was designed to evolve in order to take advantage of new technology and changing users' requirements.

By using SDDAS, scientists can do a great deal of science without developing

new software. The only preparation necessary for using SDDAS display and analyze data is to store the data in the IDFS format. In addition to enabling space scientists to focus more readily on research, SDDAS facilitates collaborative research through its flexibility, its emphasis on interactive analysis, and its capability for providing immediate access to data in globally distributed archives.

This work was done by Carrie Gonzalez, Joey Mukherjee, and Sandee Jeffers of Southwest Research Institute for Marshall Space Flight Center. For more information, contact the Southwest Research Institute at (210) 522-2010. MFS-31327

Marshall Space Flight Center,
Alabama



END

04-30-02